Electrocorticography is superior to subthalamic local field potentials for movement decoding in Parkinson's disease

Timon Merk[1], Victoria Peterson[2,5], Witold Lipski[3], Benjamin Blankertz[4], Robert S. Turner[3], Ningfei Li[1], Andreas Horn[1], R. Mark Richardson[2,5]*, Wolf-Julian Neumann[1]*

[1]Movement Disorder and Neuromodulation Unit, Department of Neurology, Charité – Universitätsmedizin Berlin, Berlin, Berlin, 10117, Germany
[2]Brain Modulation Lab, Department of Neurosurgery, Massachusetts General Hospital, Boston, Massachusetts, 02114, USA
[3]Department of Neurobiology, University of Pittsburgh, Pittsburgh, Pennsylvania, 15213, USA
[4]Department of Computer Science, Technische Universität Berlin, Berlin, Berlin, 10587, Germany
[5]Harvard Medical School, Boston, Massachusetts, 02114, USA

*These authors contributed equally to this work

Corresponding author and Lead contact: Wolf-Julian Neumann, MD, Assistant Professor for Interventional and Cognitive Neuromodulation, Movement Disorder and Neuromodulation Unit, Charité – Universitätsmedizin Berlin, Chariteplatz 1, 10117 Berlin, julian.neumann@charite.de

Email:
Timon Merk: timon.merk@charite.de
Victoria Peterson: vpeterson2@mgh.harvard.edu
Witold Lipski: lipskiw@upmc.edu
Benjamin Blankertz: benjamin.blankertz@tu-berlin.de
Robert Sterling Turner: rturner@pitt.edu
Ningfei Li: Ningfei.li@charite.de
Andreas Horn: andreas.horn@charite.de
Robert Mark Richardson: Mark.Richardson@mgh.harvard.edu
Wolf-Julian Neumann: julian.neumann@charite.de

Abstract

Brain signal decoding promises significant advances in the development of clinical brain computer interfaces (BCI). In Parkinson's disease (PD), first bidirectional BCI implants for adaptive deep brain stimulation (DBS) are now available. Brain signal decoding can extend the clinical utility of adaptive DBS but the impact of neural source, computational methods and PD pathophysiology on decoding performance are unknown. This represents an unmet need for the development of future neurotechnology. To address this, we developed an invasive brain-signal decoding approach based on intraoperative sensorimotor electrocorticography (ECoG) and subthalamic LFP to predict grip-force, a representative movement decoding application, in 11 PD patients undergoing DBS. We demonstrate that ECoG is superior to subthalamic LFP for accurate grip-force decoding. Gradient boosted decision trees (XGBOOST) outperformed other model architectures. ECoG based decoding performance negatively correlated with motor impairment, which could be attributed to subthalamic beta bursts in the motor preparation and movement period. This highlights the impact of PD pathophysiology on the neural capacity to encode movement kinematics. Finally, we developed a connectomic analysis that could predict grip-force decoding performance of individual ECoG channels across patients by using their connectomic fingerprints. Our study provides a neurophysiological and computational framework for invasive brain signal decoding to aid the development of an individualized precision-medicine approach to intelligent adaptive DBS.

Keywords

Parkinson's disease, Deep brain stimulation, Machine learning, Neuromodulation, Basal ganglia

Significance Statement

Neurotechnology will revolutionize the treatment of neurological and psychiatric patients, promising novel treatment avenues for previously intractable brain disorders. However, optimal surgical and computational approaches and their interactions with neurological disorders are unknown. How can recent advances in machine learning and connectomics aid the precision and performance of invasive brain signal decoding strategies? Do the brain disorders treated with such approaches have impact on decoding performance? We propose a real time compatible advanced machine learning pipeline for invasively recorded brain signals in Parkinson's disease (PD) patients. We report optimal movement decoding strategies with respect to signal source, model architecture and connectomic fingerprint and demonstrate that PD pathophysiology significantly and negatively impacts movement decoding. Our study has broad impacts for the development of smart brain implants for the treatment of PD and other brain disorders.

Introduction

Subthalamic deep brain stimulation (DBS) for Parkinson's disease (PD) is one of the most successful neurotechnological advances in translational neuroscience to date. In addition to its clinical utility, DBS has provided unique insight into the neurophysiology of movement disorders (Cagnan *et al.*, 2019; Krauss *et al.*, 2021). PD has been associated with increased beta synchronization and beta bursts in the basal ganglia (Kühn *et al.*, 2006; Neumann *et al.*, 2016; Kehnemouyi *et al.*, 2021) and exaggerated phase amplitude coupling and waveform sharpness asymmetry in cortex (de Hemptinne *et al.*, 2015; Cole *et al.*, 2017). Symptom severity in the OFF medication state was shown to correlate with resting beta power in the STN across patients (Kühn *et al.*, 2006; Neumann *et al.*, 2016). Such observations have inspired the idea of adaptive DBS (aDBS), where electrophysiological signals are used to change stimulation parameters in response to evolving clinical states (Little *et al.*, 2013; Beudel and Brown, 2016; Tinkhauser *et al.*, 2017; Swann *et al.*, 2018; Piña-Fuentes, van Dijk and M, 2019; Velisar *et al.*, 2019; Hwang *et al.*, 2020; Petrucci *et al.*, 2020). In a series of seminal papers it was shown that significant clinical benefit and reduced side-effects could be achieved, when stimulation was triggered by beta power (Little *et al.*, 2013; Velisar *et al.*, 2019). Machine-learning for aDBS applications can integrate multivariate feature sets for adaptive DBS control beyond beta power. First trials on machine learning based movement classification to trigger adaptive DBS either using electrocorticography (ECoG) or subcortical local field potentials (LFP) in essential tremor have shown promising results (Opri *et al.*, 2020; He *et al.*, 2021). In the future, smart implants may become available that combine invasive brain signal decoding with real time stimulation adaptation, towards a precision medicine approach to adaptive DBS in PD and other brain disorders. However, the identification of optimal decoding strategies and the characterization of relevant factors with impact on decoding performance remains and unmet need. With the present study, we address this by a thorough investigation grip-force decoding that is motivated by the well described relationship of vigor, movement velocity, bradykinesia and dopamine in Parkinson's disease (Turner and Desmurget, 2010; Yttri and Dudman, 2016; Lofredi *et al.*, 2018). We use state-of-art machine learning algorithms with multimodal invasive neurophysiology and whole-brain connectomics in PD patients undergoing DBS electrode implantation. Our results highlight the utility of cortical vs. subcortical signals to accurately decode grip-force and establish a link between decoding performance and motor impairment in PD. Finally, we investigate brain networks from ECoG recording locations with normative structural and functional connectomics and demonstrate the predictive power of connectomic fingerprints for brain signal decoding.

Results

Real-time processing & Feature Definition

We analyzed sensorimotor ECoG and subthalamic LFP data recorded intraoperatively from 11 PD patients undergoing DBS implantation during performance of a Go/No-Go based cued grip-force task (Figure 1A). Individual electrode localizations in Montreal Neurological institute (MNI) space are shown in Figure 1B with

typical responses (Kühn *et al.*, 2004; Androulidakis *et al.*, 2007; Kondylis *et al.*, 2016; Lofredi *et al.*, 2018) in Figure 1C aligned to onset of grip force (total n=2685, on average n=244 ± 149 STD movements per patient, see Figure 1-figure supplement 1 for more detail on grip-force variability). For the use in machine learning models, band power feature time-series were extracted in a real-time BCI compatible implementation (Figure 1D) streamed in virtual packets of 100 ms length at a sampling rate of 1000 Hz to mimic the online application. Variance as a measure of amplitude of rereferenced, band-pass filtered raw data segments was extracted at 10 Hz with an adaptive window length from 1000 – 100 ms of past data for eight oscillatory features [θ (4-8 Hz), α (8-12 Hz), β (13-35 Hz), low β (13-20 Hz), high β (20-35 Hz), low γ (60-80 Hz), high frequency activity (HFA) (90-200 Hz) and all γ (60-200 Hz)]. All features were normalized to the median of the past 10 seconds to compensate for potential signal changes over time. The target variable was continuously measured grip-force (z-scored for each recording session), which was cleaned from noise and baseline drift (Xie, Schwartz and Prasad, 2018).

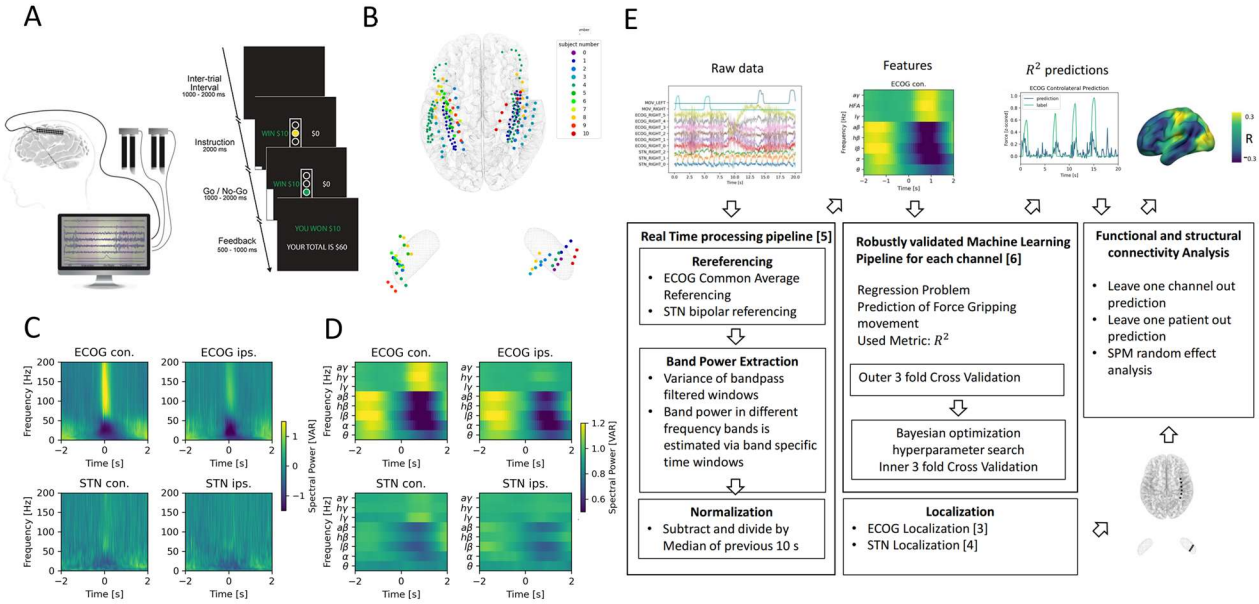

Figure 1: Movement induced spectral changes are more dominant for ECoG than STN-LFP signals for a grip force task before and after a machine learning feature signal processing pipeline.
(A) ECoG, STN and gripping force were recorded simultaneously during performance of a Go / No-Go task. (B) Individual ECoG and STN electrodes were localized and transformed into in Montreal Neurological Institute (MNI) space. Note that ECoG strip designs varied slightly between patients (see Supplementary File 1a), leading to varying dimensions of overall input feature matrices. The number of ECoG channels (average n= 9.45 ± 11.15 STD per hemisphere) is higher compared to the number of STN LFP channels (n=3). (C) Mean spectral power of all ECoG and STN channels for contra- and ipsilateral movements showed typical movement induced spectral changes. (D) Virtual streaming of data packets secured real-time compatible processing and normalization to extract time-frequency modulations into discrete feature time-series. Mean features of all ECoG and STN channels are visualized. (E) Schematic flow chart of the implemented real-time enabled feature extraction, machine learning evaluation and functional and structural connectivity analysis pipeline.

Including preceding signals up to 500 ms before the decoded sample improves grip-force decoding performance

A linear model analysis of all eight oscillatory features per channel was used to investigate the contributing band power correlations for time-points simultaneous to and preceding target samples of continuous grip-force measurements. Figure 2A shows the weight distributions of multivariable linear models of the best performing channels per subject. Since each cortical or STN electrode has multiple channels, only the best channel per electrode is selected for this visualization. As the interpretability of coefficients in multivariable models is limited (Haufe *et al.*, 2014) we have further visualized the normalized coefficients of univariate models for each relative time-point and frequency band in Figure 2B. Next, to investigate the cumulative performance contribution of preceding time points for optimal feature construction, all frequency bands were concatenated while continuously increasing the cumulative number of premovement time-points (from -100 to -1000 ms) and each set was subjected to training a Wiener Filter. The respective best channel R^2 performances are shown in Figure 2C. A performance saturation becomes visible when concatenating 5 time-points from 500 ms (prior to target sample) to 0 ms (target sample), resulting in an optimal input vector of 8 frequency bands with 5 time-points (= 40 features) for further analyses.

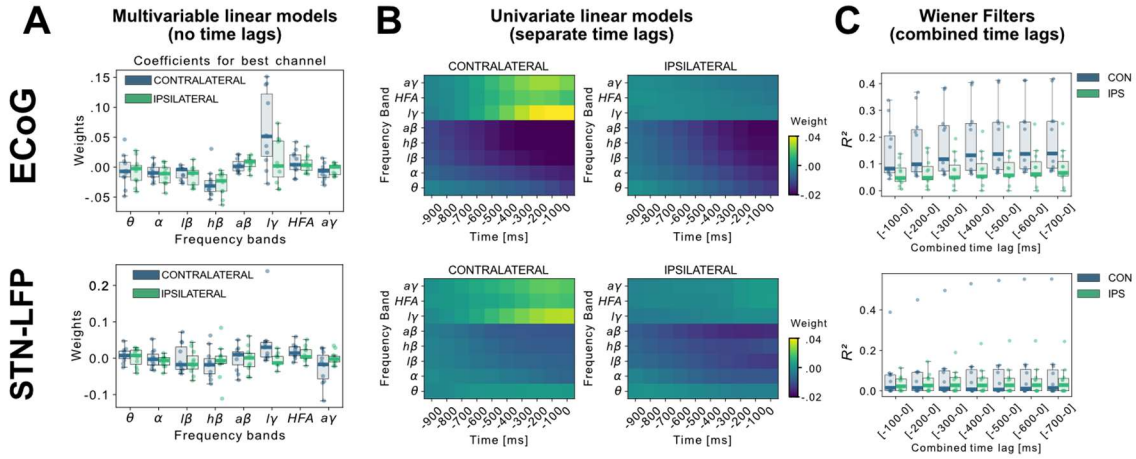

Figure 2: Linear Models and Wiener Filters reveal temporally and spectrally specific coefficient distributions with grip-force decoding performance gain by including signals preceding the target sample by up to 500 ms. Multivariable linear model coefficients trained only from the instantaneous sample (0 time lag with respect to decoded target sample) including all frequency bands from best channels per patient resemble movement induced spectral changes with beta desynchronization and gamma synchronization (A). ECoG derived coefficients yield higher absolute values than STN-LFP derived coefficients. (B) Univariate frequency and time lag specific Linear Models were trained and visualized to improve interpretability of average coefficients in the absence of interactions. Low γ (60 - 80 Hz), HFA (90 - 200 Hz) and all γ (60 – 200 Hz) bands show stronger positive associations for contralateral over ipsilateral movements. Moreover, stronger associations are visible for ECoG over STN-LFP signals for β, HFA and γ bands. (C) Wiener Filters can integrate multiple time-steps in Linear Models leading to an incremental performance gain when signals are included preceding the current target sample by up to 500 ms.

XGBOOST outperforms other machine learning models for grip-force decoding

In order to build a grip-force decoder, different machine learning (ML) algorithms were tested in a large-scale Bayesian Optimization hyperparameter search (see Supplementary File 1B for a list of hyperparameters for each model). Elastic - Net regularized Linear Models, Neural Networks and Gradient Boosted trees (XGBOOST) (Chen and Guestrin, 2016) were tested for each channel for contra- and ipsilateral movements. XGBOOST was included as it can learn non-linearities and has advantages over other models with respect to feature selection. To further utilize potential information derived from spatial patterns, the Source Power Comodulation (SPoC) framework (Dähne *et al.*, 2014) was used in combination with Elastic - Net or XGBOOST predictors. Each model was informed by 40 features (8 specific frequency bands concatenated at 5 time-points ranging from t = -500 ms to t = 0 ms to the target sample) per channel and evaluated via rigorously cross-validated test-set predictions ranked by R^2 coefficients of determination. Figure 3 shows performance outcomes for the different machine learning methods, with overall best results achieved by XGBOOST from ECoG signals (see Supplementary File 1c for further details). Contralateral ECoG strips had significantly higher decoding performances than ipsilateral ones (contralateral R^2=0.31±24, ipsilateral R^2=0.13±0.16, p = 0.02). Given the relatively low decoding performances for STN-LFP, we applied permutation tests to confirm that performance was above chance (contralateral p = 0.025, ipsilateral p = 0.028). Corroborating the model choice in previous literature, highest STN performances were achieved with the Wiener Filter method for contra- and ipsilateral movements (Shah *et al.*, 2018). Importantly, varying combinations of multiple ECoG and/or STN channels did not lead to significant performance advantages (Figure 3C+D), which is important for the utility and design of machine learning enabled implantables.

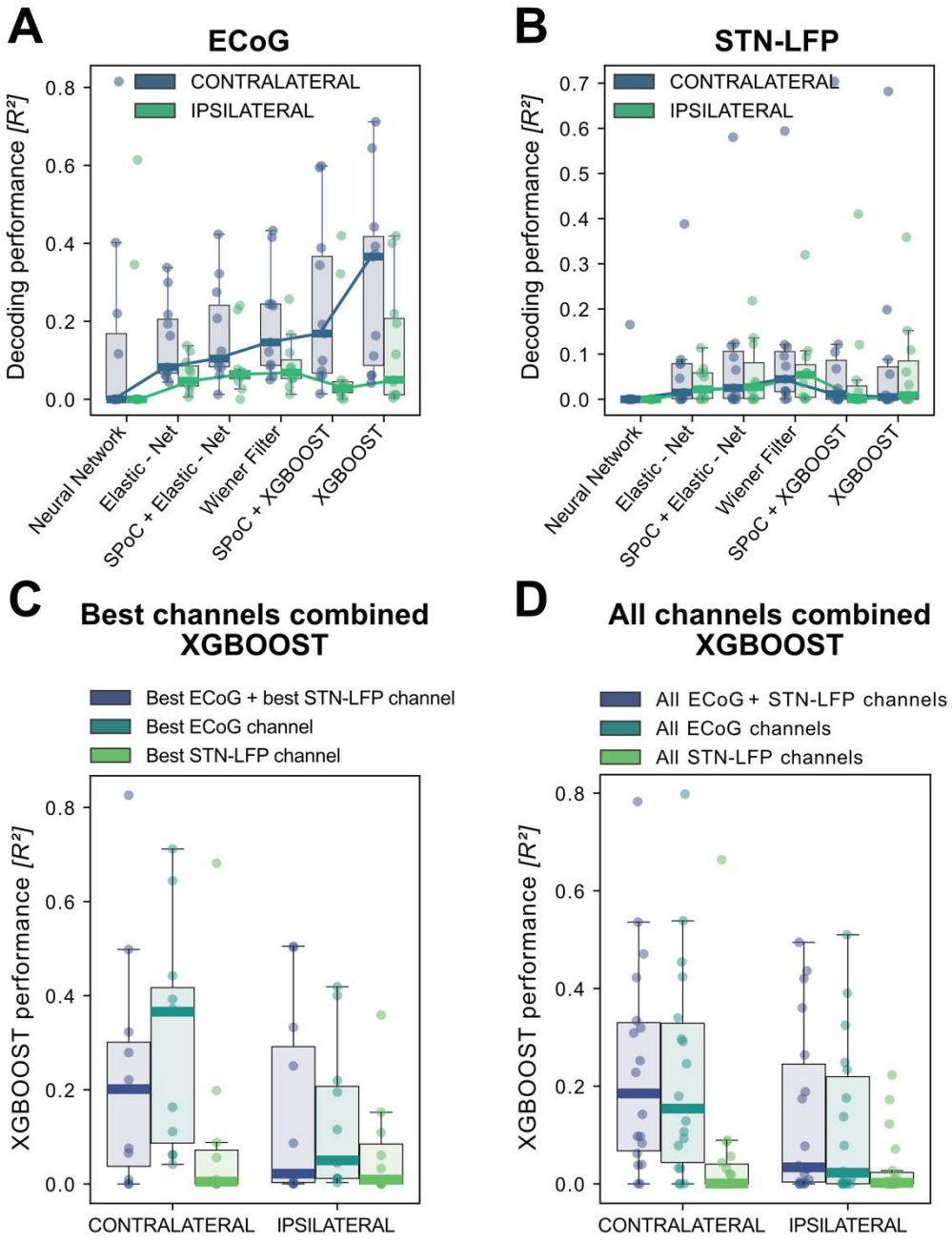

Figure 3: XGBOOST outperforms other machine learning methods for ECoG based grip-force decoding. Based on the presented real-time compatible signal processing pipeline Neural Networks, Elastic - Net regularized Linear Models, Wiener Filters and extreme Gradient Boosting (XGBOOST) regression models were tested. Mean R^2 test-set grip-force decoding performances are shown for the best channel per patient after 10 rounds of Bayesian Optimization of hyperparameters with nested cross-validation for ECoG (A) and STN-LFP (B). The same pipeline was subjected to spatial feature extraction approach using all available channels of an electrode for each patient with Source Power Comodulation (SPoC). Best ECoG (A) performances were obtained by XGBOOST regressors. STN-LFP signals (B) did not exhibit performance gain when applying advanced machine learning methods. The mean ECoG vs. STN XGBOOST performance differences of contralateral ΔR^2= 0.21 ± 0.18 and ipsilateral ΔR^2= 0.069 ± 0.08 movements,

indicate the higher grip-force decoding performance of ECoG over STN signals. The mean test-set prediction performances were higher for ECoG than for STN-LFP signals across all patients, for both contra- and ipsilateral movements. Best ECoG channels outperformed best STN-LFP channels and the combination of best channels from both ECoG and STN-LFP (C). When combining multiple channels, performances improve through the combination of ECoG and STN-LFPs (D), but the performances remain below individual best ECoG channels as depicted in (C). For combined ECoG + STN – LFP training, the model learned specific combinations between both feature locations and failed to select only the best ECoG features due to overfitting.

Grip-force decoding performance is correlated with PD motor impairment and subthalamic beta burst dynamics

To investigate potential sources of bias from patient specific information on grip-force decoding performance, we performed Spearman's correlations with the grand average from all contra -and ipsilateral decoding performances. Averaging was necessary to obtain one value per patient. Age (ρ = -0.16, p = 0.32), disease duration in years (ρ = 0.31, p = 0.17) and number of movements (ρ = -0.41, p = 0.11) and movement variability (Rho = -0.49, p = 0.06) did not reveal significant correlations. We further investigated whether motor impairment related to the hypodopaminergic state in PD can explain differences in grip-force decoding across patients. Therefore, we correlated preoperative OFF medication total UPDRS-III scores, which revealed negative correlations for best ECoG (ρ = -0.55, p = 0.039) and STN-LFP (ρ = -0.55, p = 0.042) channels (Figure 4A+B). Combined ECoG and STN channel performance also showed significant correlations (ρ = -0.54, p = 0.045), as well as combined ECoG (ρ = -0.55, p = 0.045) and combined STN-LFP performances (ρ = -0.61, p = 0.024). To test whether the correlation measure was corrupted by outliers, we repeated the analysis using the robust percentage-bend correlation (Pernet, Wilcox and Rousselet, 2013) which replicated the significant association between UPDRS total score and mean contra -and ipsilateral channel performance for ECoG (r = -0.62, p = 0.04) and STN (r = -0.7, p = 0.016). This correlation was temporally specific to decoding of ongoing grip-force, indicative of the models' underestimation of motor output (Figure 4C). Thus, the lower decoding performance in patients with more severe symptom severity could not be attributed to changes in decoder output in the absence of movement or temporal imprecision. This has practical implications and highlights the importance of investigating interactions between disease and machine learning approach for neural implants.

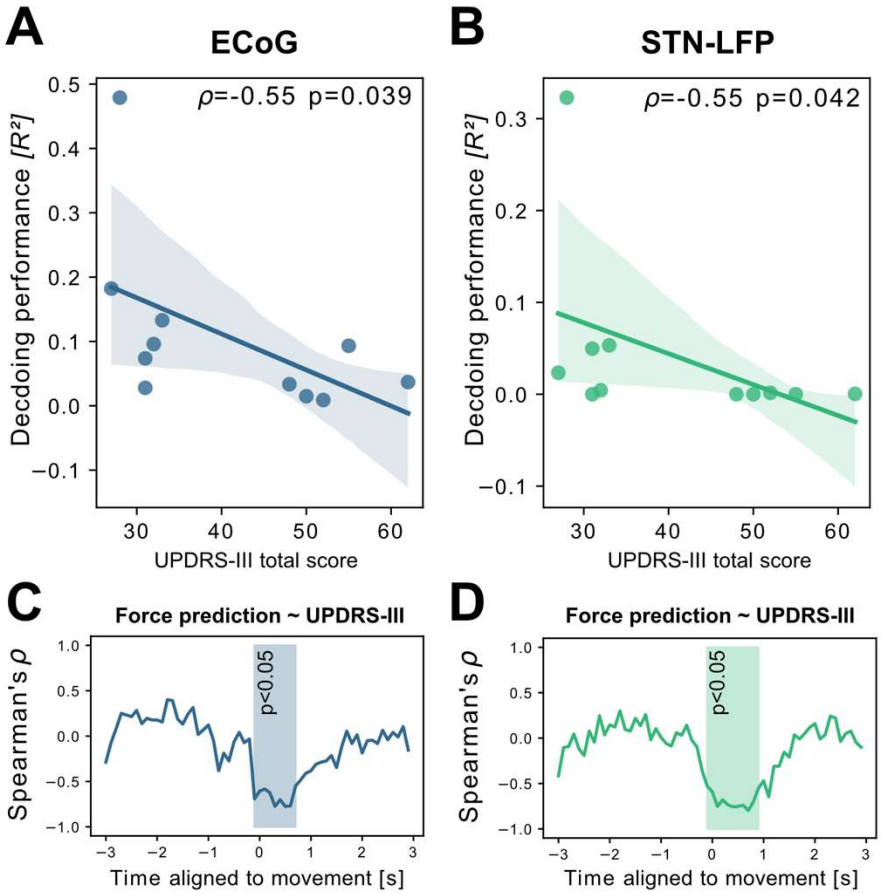

Figure 4: Grand average grip-force decoding performances correlate inversely with preoperative PD motor sign severity. UPDRS-III scores show significant negative correlations with patient-wise XGBOOST grip-force decoding performance averages for (A) ECoG (ρ = -0.55, p = 0.039) and (B) STN-LFP signals (ρ = -0.55, p = 0.042). The temporal specificity of this correlation is revealed through movement aligned sample-wise correlations of average force prediction model output with UPDRS-III scores across patients (cluster based corrected significant segments are displayed shaded) (C+D).

To better understand the relationship of PD pathophysiology and grip-force decoding performance we have further investigated associations between cortical and subthalamic beta burst dynamics. We follow the methodology of previous reports that demonstrated that the time spent in beta burst correlates with impairment of movement kinematics (Torrecillos *et al.*, 2018). Beta bursts were defined as threshold crossings of the beta feature vector above the 75th percentile of the baseline period. Following the previous finding that specifically the time-spent in low-beta but not high-beta bursts was correlated with PD motor impairment (Lofredi *et al.*, 2019), we investigated these bands separately for the motor preparation period (-1 to 0 s with respect to movement onset) and movement execution period (0 to 1 s following movement onset). To uncover a potential relationship of the beta-burst metric with PD pathophysiology, we performed correlations with UPDRS-III total scores. Significant correlations were found between UPDRS-III and low-beta bursts in STN-LFP signals during motor preparation (ρ = 0.63, p = 0.02; Figure 5A) and movement

243 execution (ρ = 0.56, p = 0.04; data not shown), but not for the high-beta band (p>0.05). Conversely, for
244 ECoG high-beta but not low-beta burst dynamics during motor preparation but not movement periods were
245 significantly correlated with UPDRS-III total scores (ρ = 0.55, p = 0.04). In summary, we provide evidence
246 that both subthalamic and cortical beta burst dynamics relate to PD motor sign severity with subthalamic
247 low-beta bursts showing the most robust correlations, both during motor preparation and movement periods.
248 To relate these findings to movement decoding performance from cortex, we correlated the grand average
249 XGBOOST grip-force decoding performances from ECoG channels (as above for UPDRS-III) with high- and
250 low-beta burst dynamics in both ECoG and STN-LFP signals. ECoG based grip-force decoding performance
251 was significantly correlated with subthalamic low-beta burst dynamics during motor preparation (ρ = -0.76,
252 p = 0.004) and movement execution (ρ = -0.71, p = 0.005; Figure 5B). Subthalamic burst dynamics in the
253 high-beta band also correlated with ECoG decoding performances during movement (ρ = 0.71, p = 0.007)
254 but not motor preparation. Cortical burst dynamics from ECoG signals did not reveal significant correlations
255 with ECoG based grip-force decoding performances. Relevant correlations alongside exemplar burst
256 visualizations and corresponding grip-force decoding traces are shown in Figure 5.

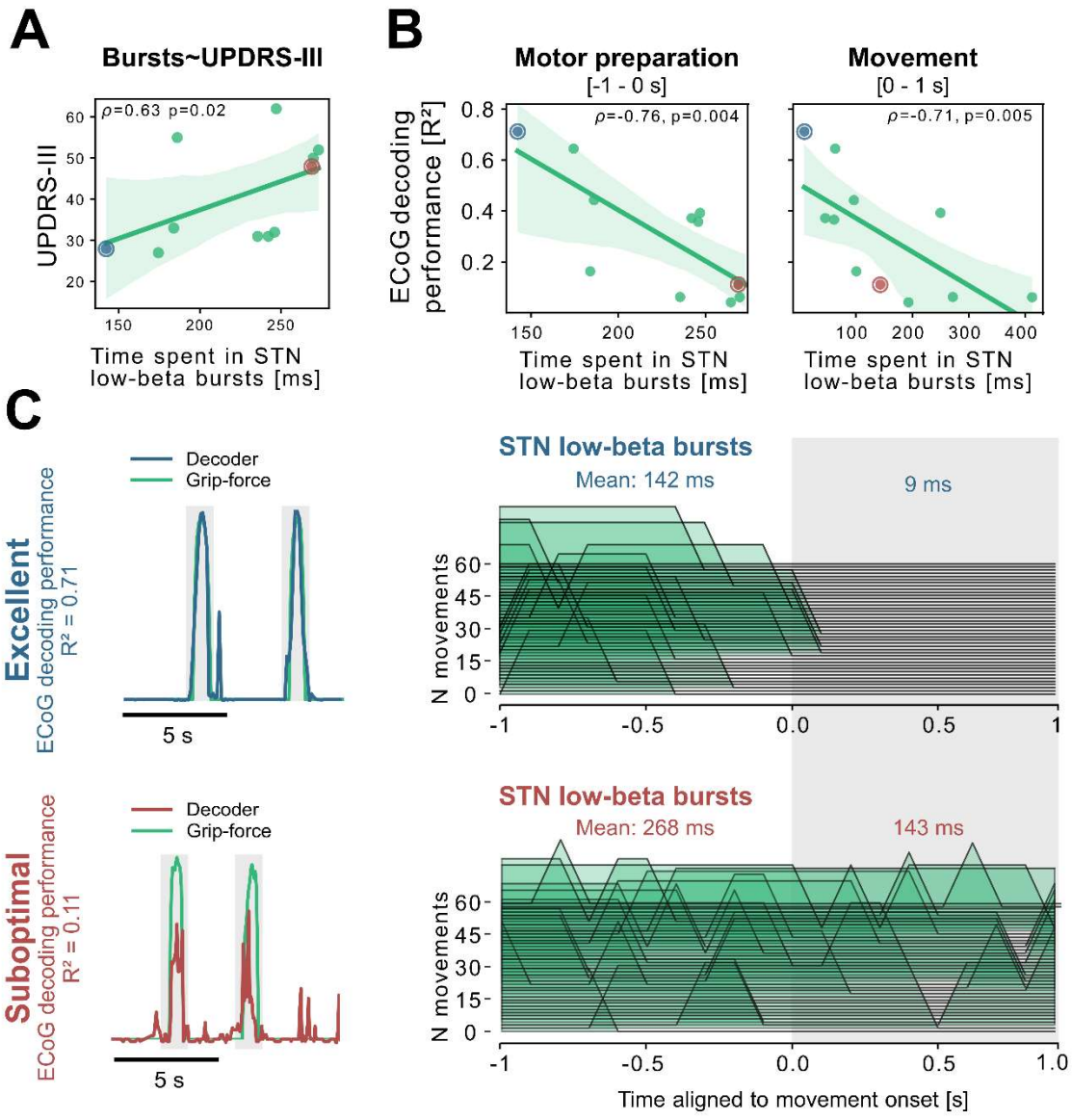

Figure 5: Subthalamic low-beta bursts relate to PD motor impairment and are associated with lower ECoG decoding performance. UPDRS-III scores are significantly correlated with time spent in subthalamic low-beta bursts in the motor preparation period (A) and during movement (not shown). Average XGBOOST decoding performance correlated inversely with time spent in subthalamic low-beta bursts during motor preparation and movement performance (B). Patient examples with excellent (R^2 = 0.71; blue) and suboptimal (R^2 = 0.11; red) performances are highlighted in (B) and shown in further detail in (C). Note the difference in decoder output with respect to the original grip-force trace (left panel) and the differences in burst frequencies and durations across movement repetitions (right panel) in the motor preparation and movement execution (grey shaded area) period.

Brain mapping of grip-force decoding performance from invasive cortical and subthalamic recordings

The spatial distributions of decoding performance on cortex and STN for contra- and ipsilateral movements are shown in Figure 6. To evaluate the relevance of recording location with respect to decoding performance, we calculated correlations of performance measures with a priori defined implantation targets, namely the dorsolateral STN (Caire *et al.*, 2013; Horn, Kühn, *et al.*, 2017) and the hand-knob of the precentral gyrus (Mayka *et al.*, 2006). Linear mixed effects models showed a significant within-subject relation for contralateral ECoG decoding performances (β=-0.002, Lower CI=-0.003, upper CI=-0.001, R^2= 0.57, p<0.001), but not STN locations (p > 0.05). The dependent variable was the decoding performance, the fixed effect was the distance to hand knob area or dorsolateral STN respectively, and the random effect the subject. Repeating the analyses across electrodes and patients in a cross-validated manner revealed no significant predictive value (p > 0.05). Thus, Euclidean distance to hand knob area for ECoG and therapeutic target for STN was significantly correlated with decoding performance within patients, but could not predict decoding performance across channels or patients.

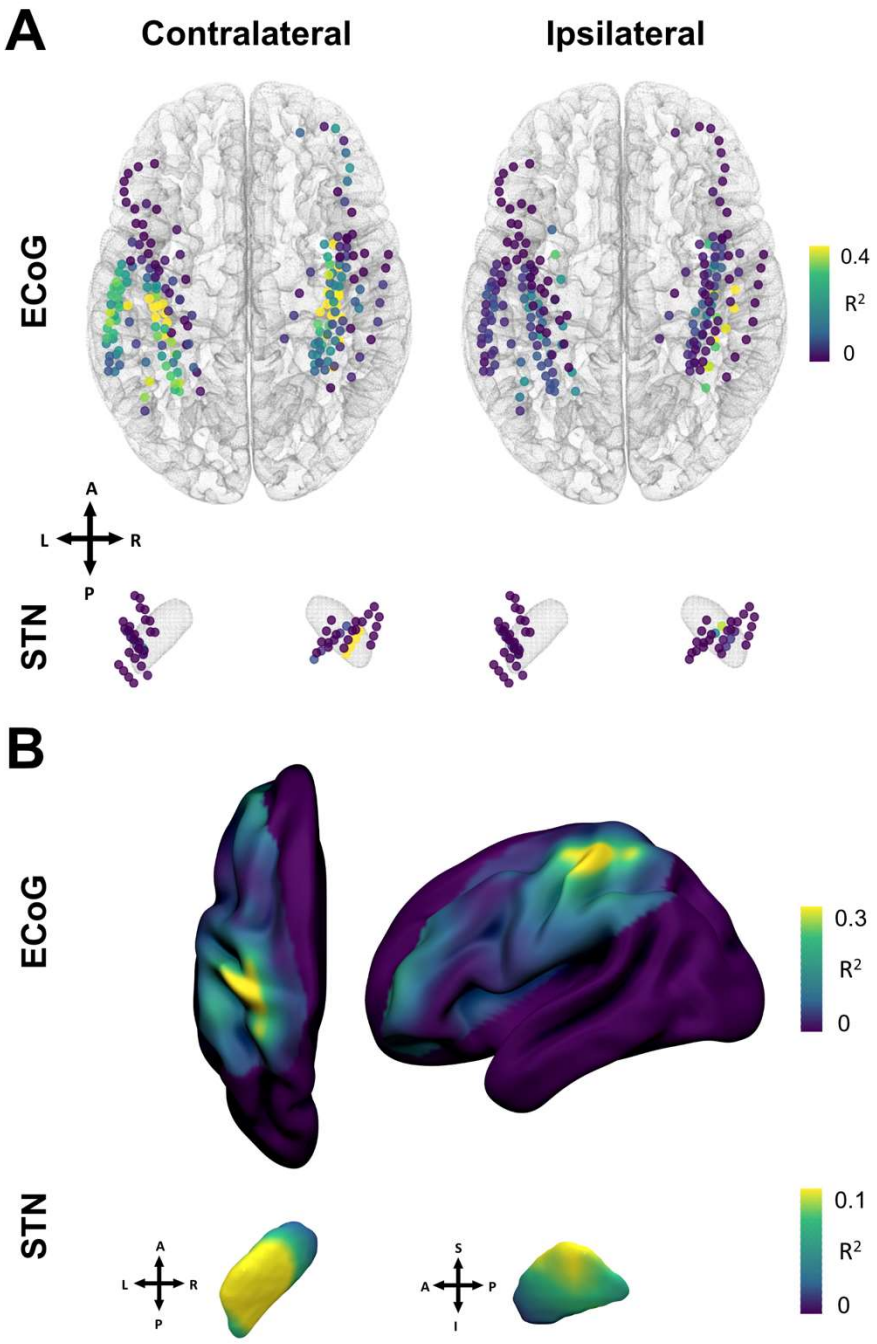

Figure 6: Grip-force decoding performances spatially peak in sensorimotor cortex and the dorsolateral STN. (A) Channels are color coded for individual XGBOOST grip-force regression performances per channel. Performance differences shown are in favor of ECoG over STN and contralateral over ipsilateral recording locations for movement decoding. (B) Spatial interpolation across all contacts projected to the left hemisphere shows peak performances in sensorimotor cortex. STN interpolated decoding performance peaks in the dorsolateral portion of the STN, in proximity to the best therapeutic target (Caire *et al.*, 2013).

Whole-brain connectomics can aid the discovery of brain networks underlying the neural encoding of grip-force

The ability to account for decoding performances for invasive electrodes may soon become as important as accounting for variance in stimulation effects, as bidirectional clinical brain computer interfaces will rely both on electrical sensing and stimulation. Recently, network mapping of neurostimulation targets has shown utility to predict variance in clinical outcomes following DBS (Horn, Reich, *et al.*, 2017; Horn and Fox, 2020; Li *et al.*, 2020). Here, we extended the same framework to predict variance in grip-force decoding performance observed from single channels, using the XGBOOST grip-force decoding results. In this approach – termed *prediction network mapping* – we calculated functional and structural connectivity *fingerprints* by projecting each recording location to a group connectome that was acquired in a cohort of PD patients. These fingerprints denote to which other brain areas each site is connected to. Using a discriminative fiber tracking analysis, (Baldermann *et al.*, 2019; Li *et al.*, 2020) we analyzed the predictive value of structural connectivity from ECoG recording locations (for an exemplar case see Figure 7A) for XGBOOST decoding performance. Therefore, diffusion imaging derived whole-brain fiber connectome data traversing to more than 20% of recording locations were used (Figure 7B). The specific fiber distributions included structural projections spanning sensory, motor and prefrontal cortex, and could significantly predict decoding performance of left out channels ($\rho = 0.38$, $p < 0.0001$; thresholded at a false discovery rate $\alpha = 0.05$) and patients ($\rho = 0.37$, $p < 0.0001$) in a cross validated manner (Figure 7D). Next, we created spatial models of optimal decoding performance for functional connectivity (R-Maps are shown in Figure 7C). This model led to significant predictions of decoding performance in leave-one-channel-out ($\rho = 0.37$, $p < 0.0001$) and leave-one-subject-out cross validations (functional connectivity $\rho = 0.37$, $p < 0.0001$) (Figure 7E). The results were further validated with voxel-wise correlations using the statistical parametric mapping (SPM) framework (see methods for further details). Models such as the two presented here could be generalized to all BCI applications and used to identify brain networks that encode specific behavioral and clinical target variables.

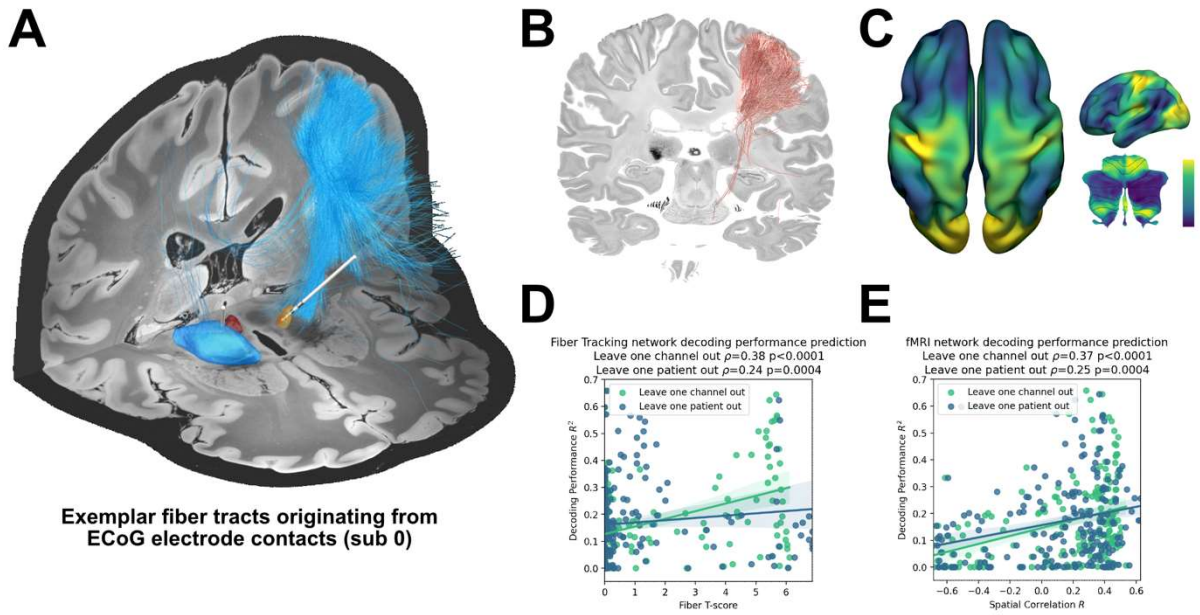

Figure 7: Structural and functional movement decoding network analysis reveals cerebellar as well as sensorimotor cortical decoding capacity. (A) Visualization of fibers originating from the ECoG recording locations of subject 1. (B) Decoding performance across all subjects and channels significant fiber tracts are displayed. All ECoG contacts were projected to the left hemisphere. For every fiber a t-test statistic between connected and unconnected brain regions was calculated. Only significant fibers, indicating structural connectivity to grip-force decoding performance, are shown. (C) The optimal R-Map is shown for the cortical surface as well as cerebellum for fMRI functional connectivity. Fingerprints were calculated between the functional connectivity of every electrode contact to all other voxels. The R-Map was then calculated as a correlation between individual contact fingerprints and the contact specific R^2 decoding performance. (D) Fiber tracking connectivity predicts grip-force decoding performance (leave one channel out cross validation ρ = 0.38, p < 0.0001, leave one patient out cross validation ρ = 0.24, p = 0.0004). Here each individual point represents a statistic of connected and unconnected fibers of each contact or patient. The previously calculated fiber statistic within each cross-validation fold could thus predict the channel or patient specific performance. (E) Functional connectivity predicts decoding performance (leave one channel out cross validation ρ = 0.37, p < 0.0001, leave one patient out cross validation ρ = 0.25, p = 0.0004). The spatial correlation between individual fingerprints and the cross-validation specific R-Map, predicts left out decoding performances.

Discussion

Bidirectional brain computer interfaces will revolutionize the treatment of previously intractable brain disorders with brain signal decoding based adaptive neuromodulation. DBS provides a unique platform to trailblaze neurophysiological approaches, disease specific modulation and computational strategies for brain signal decoding for next-generation brain implants. Here, we investigated clinical and computational strategies for grip-force decoding as a representative and pathophysiologically relevant behavioral target variable. We used multimodal invasive neurophysiology time-series data in PD patients undergoing DBS electrode implantation. Our findings can be broken down into four advances to the field: 1) we developed a

new decoding approach based on multispectral time-concatenated band-power measures, subjected to Bayesian optimized extreme gradient boosted ensembles (XGBOOST): this outperformed traditional linear model-based methods and may be generalized to all brain signal-based regression problems. 2) Next, we demonstrate that electrocorticography signals outperform subthalamic LFP for grip-force decoding, supporting the utility of additional ECoG in adaptive DBS research for PD patients. 3) Our findings link PD motor impairment, PD pathophysiology with deterioration in decoding performance, highlighting a potential impairment in movement coding capacity through subthalamic low-beta bursts during motor preparation and execution periods. 4) Finally, we could significantly predict how well a specific recording site would perform to decode grip force based on brain connectivity. This novel framework (termed prediction network mapping) can be used in future implants to identify connectomic networks from which brain sensing can predict symptoms and behavior.

Limitations

Our analysis is retrospective in nature and the data were obtained in context of a Go/No-Go task, which may have implications on the generalizability of the findings in the application during naturalistic behavior. All model training and evaluations were conducted offline. Nevertheless, we took meticulous care to exclude any circularity in processing and machine learning applications. To this date, such circularities are overlooked in some movement decoding papers with filtering, normalization and time frequency transformation across entire sessions, thus reaching into the future from the point of the individually decoded sample. Ridding our analysis from data that would be unavailable in a real-time setting as reported in this study, leads to worse performances, but gives a more realistic estimate of model performance in the clinical use-case. While gripping is a relevant motor skill for human behavior, our findings are restricted to the decoding of grip-force and may have limited generalizability to other movements. The overall number of patients in this study is low. This may have limited a more detailed analysis of bias and other factors, beyond the described correlation of clinical symptom severity, subthalamic beta burst dynamics, electrode location and connectomics. Most importantly, the signal to noise ratio may further impact decoding accuracies differently for ECoG and LFP signals. This could in part explain why decoding from ECoG signals may benefit more from complex and non-linear model architectures. The comparability of ECoG and LFP recordings was further affected by the higher number of available ECoG channels, when compared to only three bipolar LFP channels. However, the large effect size of superior decoding performances with ECoG may indicate that this bias does not relevantly impact the interpretation of our findings. An additional limitation was the relatively small amount of available data per patient, which was constrained by the intraoperative setting (see Table 1). For deep learning approaches we expect better performances with increased dataset sizes, which may become available, either through externalized extraoperative recordings (He *et al.*, 2021) or sensing enabled implantable devices (Opri *et al.*, 2020; Gilron *et al.*, 2021). Importantly, our finding that decoding performances from single contacts outperform multi-electrode models may be a consequence of a combination of short recording durations in this study, suboptimal computational model

selection and the fact that sensorimotor cortex and STN are part of the same circuit that is synchronized in oscillations. While we have made an effort to accommodate models that are optimized for spatio-spectral feature learning, and we are confident that these cannot outperform single channel approaches in this dataset, future studies should cautiously reinterrogate this issue in larger datasets, e.g. by implementing neural networks optimized for this purpose (Peterson et al., 2021). Finally, we should acknowledge that the exploration of the neural feature space in this study was non-exhaustive, and further raw data features, such as the local motor potential (Mehring et al., 2004), waveform shape features (Cole and Voytek, 2017) and aperiodic signal components (Wilson, Castanheira and Baillet, 2022) could further improve decoding performances in future movement decoding studies.

Decoding grip force based on invasive electrophysiology

Our study defines a novel computational strategy to decode grip-force based on ECoG and LFP in patients undergoing DBS for PD. It explores defined oscillatory feature sets and compares machine learning models with varying complexity, from linear models to artificial neural networks and regression trees. ECoG based movement decoding of varying movement types has been previously investigated in epilepsy patients that underwent electrophysiological monitoring (Leuthardt *et al.*, 2004) through which local motor potentials and gamma band activity were highlighted as informative features (Gunduz *et al.*, 2016). First analyses based on STN-LFPs in PD patients have shown that Wiener Filter architectures can be successfully used for grip-force decoding (Tan *et al.*, 2016; Shah *et al.*, 2018). The present study extends these previous reports to a continuous non-trial-based decoding approach. Furthermore, a direct comparison of ECoG and LFP performance with relation to systematic machine learning methods was lacking. Our findings indicate that sensorimotor ECoG recordings are more informative than LFP recordings from the STN for grip-force decoding. While this finding is robust, we should acknowledge that the size and shape of electrodes (see Supplementary File 1a) and the spatial orientation and size of the neural architectures that are sampled are not directly comparable across these methods. Thus, it is difficult to derive the relative importance of the different brain regions for grip-force and vigor processing in motor control from this comparison. Instead, we interpret our result as a practical demonstration of the greater utility of ECoG signals for movement decoding. The results in this study are based on extracted band-power features and show superior performances with XGBOOST, when compared to other model architectures and algorithms. More specifically, best performances were obtained for Bayesian optimized XGBOOST models trained on data from single ECoG channels without additional benefit from channel combinations or combined ECoG and STN channel sets. In the future, this machine learning approach can be adopted to extend the clinical utility of invasive brain stimulation approaches for other brain disorders, e.g. through decoding of tics or obsessive compulsive behavior in neuropsychiatric DBS indications.

Towards machine learning based adaptive stimulation in Parkinson's disease

Adaptive DBS (aDBS) has the potential for significant innovation in movement disorders (Starr, 2018). For Parkinson's disease, different control policies of subthalamic beta band activity are now tested in clinical trials to improve the treatment for patients with akinetic rigid dominant PD (ClinicalTrials.gov Identifier: NCT04681534, NCT04547712) (Little *et al.*, 2013; Arlotti *et al.*, 2018; Velisar *et al.*, 2019). Beyond subthalamic beta power, ECoG recordings were previously used to successfully decode the presence of dyskinesia through elevated levels of gamma band synchronization. This could be used to reduce stimulation intensity to alleviate medication and stimulation induced dyskinesia (Swann *et al.*, 2018). Such single biomarker approaches have the advantage that pathophysiological mechanisms may be the direct target of intervention, while machine learning based decoding methods derive correlates of symptoms and behavior indirectly through learning potentially noisy correlations (Neumann *et al.*, 2019). Therefore, single biomarker based aDBS presents an optimal starting point for investigating the clinical utility of aDBS in controlled study designs. However, single biomarkers alone cannot account for the diverse and complex set of clinical signs of PD and behavior, e.g. during gait (Molina *et al.*, 2021; Thenaisie *et al.*, 2022), speech and tremor (Hirschmann *et al.*, 2013, 2017). Here a versatile decoding based control algorithm may further improve clinical outcome for these patients in the future (Neumann *et al.*, 2019; Merk *et al.*, 2022). Indeed, machine learning-based decoding has been successfully described in first translational breakthrough studies (Opri *et al.*, 2020; Gilron *et al.*, 2021; He *et al.*, 2021). In a complementary approach, we focused on direct grip-force decoding, motivated by the hypothesis that future aDBS studies increasing DBS amplitude during periods of higher movement vigor may advance the successful treatment of bradykinesia in PD. While our previous findings indicate that relative amounts of beta can still signal bradykinesia during movement, (Lofredi *et al.*, 2019; Feldmann *et al.*, 2021) further positive control parameters could keep stimulation proportional to intended movement vigor. Moreover, recent reports that beta power correlates negatively with phasic dopamine release may further substantiate the idea of movement/kinematics based STN stimulation to support intrinsic movement related dopamine signals (Schwerdt *et al.*, 2020). We may speculate that DBS constitutes a network modulation that is similar to dopamine transients by suppressing local firing of the subthalamic nucleus (Milosevic *et al.*, 2018) and shifting the balance of basal ganglia from indirect to direct pathway activity. As highlighted above it was recently shown in non-human primates that phasic decreases in beta in the basal ganglia are correlated to phasic dopamine signals during movement (Schwerdt *et al.*, 2020). Thus, in order to support the intrinsic dopaminergic capacity of PD patients, future machine learning based aDBS approaches could be complemented by algorithms that inform the stimulation on behavioral and motor adjustments to mimic intrinsic phasic dopamine signals. Previous studies have successfully decoded the presence of movement using cortical beta activity (Opri *et al.*, 2020) which could also become a viable treatment option in PD. However, getting an estimate of movement vigor i.e. through the prediction of grip-force may complement advanced aDBS control policies, as multivariate models emerge for the next-generation of neurotherapeutics.

Notably, the proposed adaptive stimulation would require a fast algorithmic adaptation of stimulation to ongoing behavior. This could be combined with additional slower adaptations in response to medication or sleep cycles. Specifically for PD, beta activity based adaptive stimulation can be well suited to track the patient's overall symptom state (Tinkhauser and Moraud, 2021) while more rapid stimulation adaptations based on vigor can follow fast kinematic changes. The utility of vigor-based stimulation and the combination of this approach with additional slower adaptation algorithms, require further proof-of-concept studies before the clinical utility can be foreseen. In our study, we demonstrate that motor symptom severity itself can have direct and negative effects on decoding performance, which we should keep in mind during clinical decision making. Previous studies have shown that the presence of beta bursts correlated with motor performance in cortex (Little *et al.*, 2019) and STN (Torrecillos *et al.*, 2018), which could degrade decoding performance (Khawaldeh *et al.*, 2020). Our study replicates and extends these findings, as we show a direct correlation between movement related beta burst dynamics and PD motor sign severity. More importantly, our results show that the amount of time the STN is bursting in the low-beta band, during motor preparation and movement execution is inversely correlated with ECoG based grip-force decoding performance. An obvious interpretation of this finding is that excessive synchronization in the STN may impair flexible motor control by decreasing information coding capacity and neural entropy as previously suggested in animal studies (Mallet *et al.*, 2008; Cruz *et al.*, 2009) and recently suggested for subthalamic beta bursts (Velasco *et al.*, 2022). Again based on the inverse relationship of beta activity and dopamine (Schwerdt *et al.*, 2020), we may speculate that beta bursts may relate to transient dips in dopamine signaling. Dopamine was shown to precede and invigorate future movement (da Silva *et al.*, 2018). If subthalamic beta bursts indicate phasic decreases in dopaminergic innervation, we could expect a loss of invigoration and reinforcement of ongoing neural population activity in the cortex – basal ganglia – thalamic loop, which offers an elegant explanation for the lower decoding performance from ECoG signals in the absence of obvious cortical activity patterns. Beyond beta bursts our findings indicate general impact of motor symptoms in the hypodopaminergic state on machine learning based kinematic decoding capacity. This highlights the conceptual relevance of disease specific interactions with computational models. Interestingly, in the hypodopaminergic state, the model output underestimated the grip force extent produced by the patients. This could reflect a loss of neural vigor representations related to insufficient dopaminergic modulation (Turner and Desmurget, 2010). In the future, we will have to account for the individual impact of disease specific changes in brain signals that affect decoding performance. Further, our results corroborate the notion that dopamine plays a key role in coding and modulating neural representations of movement kinematics in the human brain.

Connectomics can aid the discovery of brain networks underlying encoding of clinical and behavioral target variables

Decoding performance for clinical BCI may be drastically improved when adjusting brain signal recording sites to the underlying interconnected network that is relevant for encoding of the specific target behavior. For instance, when decoding language or speech, one could envision that recordings at either Broca's or

Wernicke's region could be helpful, but a combination of both could be optimal. The two regions form a network with direct connections via the Arcuate Fascicle. In the present study we have leveraged multisite recordings from various electrode locations across patients to identify the network that would be most informative for grip force decoding. For this endeavor, we adapted two existing methods that are able to isolate i) connected voxels and ii) connected fiber tracts (Horn, Reich, *et al.*, 2017; Li *et al.*, 2020) associated with a specific target metric (such as grip-force decoding performance in the present case). While Euclidean distance to motor target, i.e. hand knob area for ECoG and therapeutic target for STN, was significantly correlated with decoding performance within-subject, this simplistic notion could not predict decoding performance across channels or patients. Thus, proximity to landmarks alone does not reliably help the identification of optimal recording sites. Given the complexity and vast distribution of movement related brain areas, from cerebellum to frontal cortex to parietal cortex, it may not be surprising that whole-brain connectomics outperform single region of interest based distance metrics for predicting informative recording locations. The development of a connectomic identification of optimal decoding locations has important implications in clinical adoptions of BCI technology. Preoperative identification of brain networks would allow the design of optimal electrode architectures and targeted implantation to cover strategic nodes of distributed networks for decoding of clinical variables and behavior. Moreover, connectomic approaches can inform the optimal spatial feature selection of pretrained machine learning models to facilitate brain signal decoding without the requirement for individual (re-)training. Importantly, the connectomic models that we used can be trained based on multiple dimensions of input-output relationships, e.g. for decoding of behavior like grip-force, but also for decoding clinical signs, such as tremor or mood disturbances. Thus, when implanting a high-density ECoG grid, connectomic analyses can generate target specific contact combinations, e.g. focusing on primary cortex for tremor and supplementary motor area for motor intention and bradykinesia. Our results highlight the utility of whole-brain connectomics to predict machine learning-based brain signal decoding performance that can be generalized to any bidirectional clinical brain-computer interface use-case. In the future, neurosurgeons may not target individual sensing locations in isolation, but instead determine optimal implant trajectories in accordance with whole-brain connectomic fingerprints for optimal BCI performance.

Conclusion

Our analysis from PD patients undergoing DBS implantation showed that ECoG recordings outperform STN-LFP recordings for grip-force decoding throughout different machine learning methods, with XGBOOST showing the highest performance. Parkinsonian motor sign severity and subthalamic low-beta bursts were associated with loss of decoding performance, indicating a specific link between PD pathophysiology, kinematic coding capacity and motor impairment. To investigate the spatial relationship of ECoG decoding performances in the brain, we have formalized a connectomic framework that could cross-predict decoding performances across recording sites and patients, based on underlying whole brain MRI connectivity patterns. Our findings highlight the utility of ECoG for intelligent adaptive stimulation in PD, corroborate the

role of PD symptom severity in kinematic coding and pave the way for connectomic neurosurgery for machine learning-based brain signal decoding. We hypothesize that future neurotechnological treatments may have the potential to outperform traditional drug regimes, due to a key advantage in the temporal and spatial precision of therapeutic delivery towards a precision medicine approach for intelligent adaptive DBS (Neumann *et al.*, 2019; Neumann and Rodriguez-Oroz, 2021; Merk *et al.*, 2022).

Materials and Methods

Participants

The current study is based on previously published data (Alhourani *et al.*, 2020). In brief, subthalamic LFP and subdural ECoG recordings were simultaneously acquired from 11 PD patients. The patients were subjected to bilateral STN-DBS lead implantation, as proposed by standard clinical indications criteria. In accordance with protocol #PRO13110420, approved by the Institutional Review Board of the University of Pittsburgh, informed consent for all patients was obtained prior to any surgical procedure. The subject characteristics are detailed in Table 1. UPDRS Part III scores for the off-medication conditions were collected in a time period of 1-3 months prior to surgery by movement disorder neurologists. Dopaminergic medications were withheld for at least 12 hours before intraoperative testing.

Table 1: Subject characteristics

N	Gender	UPDRS total	Hemisphere	Age	Movements	Disease duration [years]	ECoG Strip Contact Number Left	ECoG Strip Contact Number Right
0	Male	28	R	60.3	128	10.7	0	6
1	Male	27	L+R	51.2	464	14	28	28
2	Male	33	L+R	53.8	213	7.2	8	8
3	Male	31	L+R	44.2	285	10.1	8	8
4	Male	32	2L+2R	63.6	381	13.1	28+8	28+8
5	Male	52	L	59.6	84	5.9	6	0
6	Male	55	L	71.6	161	1.4	6	0
7	Male	50	L	52.5	131	8.7	6	0
8	Male	62	L+R	66.8	547	9.8	6	6
9	Male	48	L	67.9	86	17.1	6	0
10	Female	31	R	69	205	10.4	0	6

Behavioral Paradigm

The behavioral task performed for this study was previously described (Kondylis *et al.*, 2016; Alhourani *et al.*, 2020; Fischer *et al.*, 2020) and it is schematically shown in Figure 1A. The task included Go/No-Go cues

with randomized inter-trial interval durations. Feedback durations were adjusted based on grip force reaction times. In the present analyses, time-series were virtually streamed as continuous data to simulate real time grip-force decoding, irrespective of task trials. Subjects were fully awake, and no anesthetic agents were administered for at least 1 hour before the task procedure. No medication was given during the task. The task paradigm was implemented using the Psychophysics Toolbox (Brainard, 1997) on a portable computer. The trials consisted of a simultaneous presentation of a yellow traffic light in the center of a screen, and a cue on one side indicating which hand the subject should use for the subsequent response of squeezing the handgrip. The cue remained on screen for 1000 - 2000 ms, followed by the traffic light changing either green or red, signaling a ‘’go cue’’ and ‘’no-go cue’’ respectively. Subjects performed the task for a cumulative total time of 10 to 25 min. As the present study focuses on grip-force decoding performance based on the electrophysiological signals, all sessions containing valid movements were merged per subject for further analysis. To validate that the used grip-force label in our data varies not only between two movement states, but constitutes a relevant regression problem with varying force amplitude and velocity, all movement maximum amplitudes and velocity traces are visualized in the *Figure 1-figure supplement 1.*

Electrophysiological Recordings

Subdural electrode strips were implanted temporarily through standard frontal burr holes located near the coronal suture and aimed posteriorly to the hand knob motor cortex region. Strip targeting has been previously described and was based on markings of stereotactically defined overlying scalp locations (Kondylis *et al.*, 2016). STN-DBS electrodes were implanted bilaterally, targeting the dorsolateral motor area of the STN. ECoG data were recorded intra-operatively using six-contact (left n = 5 patients, right n = 3), eight-contact (left n = 3, right n = 3) and twenty-eight-contact (left n = 2, right n = 2) strip electrodes. The electrode details are shown in *Supplementary File 1a* and all ECoG and STN electrodes are plotted in Figure 1B (mean number of electrode contacts were 10.18±11.29 for left and 8.9±12 for right hemispheres). A referential montage was used in which the reference electrode was placed in the scalp and a ground electrode was placed in the skin overlying the acromion process. ECoG and STN signals were filtered (0.3–7.5 kHz), amplified, and digitized at 30 kHz using a Grapevine neural interface processor (Ripple Inc.). Force signals were digitally recorded simultaneously with the ECoG and STN-LFP signals. LFPs from the STN were recorded using the clinical DBS lead (model 3389, Medtronic) from all four contacts and referenced offline in a bipolar montage. All signals were resampled to 1 kHz for offline analysis. To investigate the variability of grip-force as a potential bias for decoding performance, we calculated the variance of peak force across movement repetitions.

Electrode Localization

Subdural electrode reconstructions were obtained by aligning pre-operative MRI, intra-operative fluoroscopy, and postoperative CT. Representative images of this technique were previously shown in detail (Randazzo *et al.*, 2016). In short, the CT and MRI were co-registered using mutual information using the

SPM software library and rendered onto 3D skull and brain surfaces using Osirix (v7.5) (Rosset, Spadola and Ratib, 2004) and Freesurfer (v5.3) software packages (Dale, Fischl and Sereno, 1999), respectively. These surfaces and the fluoroscopy images were then aligned according to common points: stereotactic frame pins, implanted depth electrodes, and skull outline positions (Randazzo *et al.*, 2016). The parallax effect of the fluoroscopic images was accounted for using the obtained distance from the radiation source to the subject's skull. Succeeding the surface-to-fluoroscopic image orientation alignment, a 3D location for each electrode contact was projected from the fluoroscopic image to the cortical surface. Deep brain stimulation electrode locations were reconstructed using the advanced neuroimaging pipeline defined by Lead-DBS using default settings (Horn *et al.*, 2019). In brief, preoperative MRI and postoperative CT scans were co-registered and normalized to MNI 2009b NLIN ASYM space. Electrode artefacts were visually identified and marked to obtain MNI coordinates of DBS electrode contacts. All electrode localizations are visualized in Figure 1B.

ECoG and LFP preprocessing and feature extraction

The entire preprocessing pipeline used in the present study was optimized for real-time performance and inspired by the Berlin Brain Computer Interface (Blankertz *et al.*, 2006). Processing was performed in Python using custom code based on MNE-python (Gramfort *et al.*, 2013), mne_bids (Appelhoff *et al.*, 2019) and pybv (https://pybv.readthedocs.io/en/stable/). All raw data files were saved in the iEEG-BIDS structure (Holdgraf *et al.*, 2019). To account for baseline drifts, the force traces were cleaned using a normalization approach presented for previous ECoG finger trajectory decoding (Xie, Schwartz and Prasad, 2018). A real-time data stream of untouched electrophysiological raw data was emulated to ensure that all processing that can impact decoding is performed in a real-time compatible manner. Referencing was performed online (i.e. after streaming virtual data packets). All LFP recordings were referenced bipolarly, against the adjacent contacts (0-1, 1-2, 2-3 with contact 0 being the lowest by convention of the manufacturer). Throughout the manuscript, we adopt the clinical usage of electrodes (also named "leads") and contacts from the DBS realm. During preprocessing (in pseudo real time), we derive 3 bipolar STN-LFP channels from 4 adjacent contacts in one DBS electrode (also called "lead"). We also follow this nomenclature for ECoG, where we call the entire strip an "electrode". ECoG electrodes in our dataset can have varying number of contacts (see Supplementary File 1a). ECoG recordings were referenced by subtracting the common average of all ECoG electrodes, therefore the number of channels per ECoG electrode is equal to the number of contacts per strip. To facilitate computationally efficient real-time enabled algorithms, time frequency decomposition for the machine learning analysis was conducted by bandpass filtering in the θ (4-8 Hz), α (8-12 Hz), β (13-35 Hz), low β (13-20 Hz), high β (20-35 Hz), all γ (60-200 Hz), low γ (60-80 Hz) and high-frequency activity, (90-200 Hz) frequency bands. Overlapping broad β and γ bands were added in addition to subbands to enable the investigation of distinct interactions within these frequency bands (Figure 1C). To estimate band specific activity, different time durations were used for band-pass filtering with longer time segments for lower frequencies, and shorter time segments for higher frequencies (θ = 1000 ms, α and β bands = 500

ms, γ = 100 ms). To get an estimate of amplitude of the activity in the filtered signals, variance was extracted in intervals of 1 s in a sliding window of 100 ms resulting in a time resolution of 10 Hz. All variance estimates were normalized by subtracting and dividing by the median in a sliding window of 10 s to account for differences in impedance and proximity to the source before subjecting the data to the machine learning analysis. All features were clipped as an artifact rejection mechanism when they exceeded a normalized value of [-2 2]. The used normalization is fully compatible with a real time prediction approach, as data acquired in the future do not influence the present predictions. See figure 1E for an outline of the methods pipeline. For the purpose of visualization, Morlet wavelets (7 cycles) were used to demonstrate the entire time-frequency decomposition (Figure 1C).

Machine learning training and evaluation

A rigorous nested cross-validation approach was implemented. An outer 3-fold cross validation split the data into folds of two third training and one third test set. For each individual channel a Bayesian Optimization hyperparameter search (Frazier, 2018) was then conducted for 10 rounds using the training set only. For each round the training data was trained and tested in an inner 3-fold cross-validation with 80 percent training size. Post-hoc assessment confirmed convergence in performance after a maximum of 5 rounds in all recordings. The mean R^2 coefficient of determination of every test set estimate of the outer cross-validation was used as the performance measure as defined below:

$$R^2(y, \hat{y}) = 1 - \frac{\sum_{i=1}^{n}(y_i - \hat{y}_i)^2}{\sum_{i=1}^{n}(y_i - \bar{y})^2}$$

Since the R^2 metric can be lower than zero for predictions that are worse than constant predictions, we used a lower threshold at zero to make performances comparable for the purpose of visualization. The input features for every model were all eight previously described frequency bands. In order to test the contribution of time points preceding the decoded target sample, frequency band features of different time points were concatenated and compared with respect to their decoding performance. The present study investigated commonly used and promising linear and non-linear machine learning algorithms, specifically elastic net regularized linear models, linear Wiener filters, neural networks, gradient boosted decision trees (XGBOOST) and source power comodulation.

Linear Models

Linear models can capture underlying feature dependencies and reveal those as correlations in each weight parameter. Input features are multiplied by a weight coefficient. The dot product of the weight vector $\boldsymbol{w}$ and feature vector $\boldsymbol{x}$ is then shifted by the bias b. The feature vector in this analysis is the vector of all frequency bands for a single time point. The prediction label y is the baseline corrected gripping force. For a linear regression the activation function is linear, is defined as follows:

$$y = \boldsymbol{w}\boldsymbol{x} + b$$

To prevent overfitting, regularization in the form of l_1 and l_2 norm is commonly used. Here we tested different parameters of the elastic-net (enet) regularization(Zou and Hastie, 2005), which is a combination of the l_1 and l_2 norm specified by the regularization hyperparameters α and ρ, respectively. The objective function of the enet model follows:

$$\min_{w} \frac{1}{2n_{samples}} \|\boldsymbol{X}\boldsymbol{w} - \boldsymbol{y}\|_2^2 + \alpha\rho\|\boldsymbol{w}\|_1 + \frac{\alpha(1-p)}{2}\|\boldsymbol{w}\|_2^2$$

where $\boldsymbol{X}$ is a matrix of dimension n x m whom i[th] row is the feature vector $\boldsymbol{x}$ of size m and $\boldsymbol{w}$ is the solution vector, which, due to the l_1 sparse regularization term, most of the coefficient will be expected to be zero. For hyperparameter-search, α and ρ were both sampled from a uniform distribution ranging from zero to one. Since elastic nets are solved using gradient descent, the maximum training iteration also needs to be specified. Here an iteration number of 1000 has been used. The implementation was done using the scikit learn Python package (Pedregosa *et al.*, 2011).

Wiener Filters

Tan et al. described the use Wiener filters in the application of force estimation from STN-LFP signals (Shah *et al.*, 2018). Here the output y is a weighted sum of features in the time and frequency domain in the weight matrix $\boldsymbol{W}$. I frequency band features are used together with J lags. For the regression analysis the activation function is kept linear, as follows:

$$y(n) = \sum_{j=0}^{J}\sum_{i=0}^{I} w_{ij}x_i(n-j)$$

This equation has a closed form solution, known as the normal equation (Proakis and Monolakis, 1996). Wiener filters essentially implement a multivariable linear model with multiple time-steps. Using Wiener filters we tested the contribution of different concatenated time-steps of brain signals preceding the decoded target sample. This provides insight about the optimal feature length in the time domain.

Neural Networks

We have further investigated the utility of artificial neural networks. While linear models and Wiener filters may underfit the data, neural networks can be very complex and have a higher risk to overfit with increasing complexity. The ideal model architecture finds a balance between under and over- fitting to the training dataset. In this context not only single weight correlations of band features could contribute to force decoding performances, but a richer representation of feature invariances in combinations of different frequency bands may be learned by additional layers and units of the model. The architecture of neural networks is derived from linear models with non-linear activation functions, which are referred to in this context as units. Multiple units are combined in different layers with different activation functions.

Explicitly, the output y of the i[th] unit in layer l is the weighted sum of activations of the previous layer units y_k^{l-1} with weights w_{ik}^l ,

$$y_i^l = f^l\left(\sum_k w_{ik}^l y_k^{l-1} + b_i^l\right)$$

Neural networks are trained through a cost function using a gradient descent algorithm. Hyperparameters were adjusted in order to prevent over -and underfitting (Geman, Bienenstock and Doursat, 1992). Here neural networks were tested with at least one hidden layer. The input nodes of this layer were in the hyperparameter search uniformly sampled in a range of 1 to 10. The number of hidden dense layers were sampled from a range of 1 to 3 layers. The hidden dense layer neurons were uniformly sampled in a range of 1 to 10. Sigmoidal and hyperbolic tangent activation functions were tested in the hidden layers. After each hidden layer a batch normalization layer and a dropout layer with a factor of 0.2 was added. The output activation function was set linear. The used training algorithm was the Adam optimizer (the learning rate was sampled from a log uniform distribution from 0.0001 to 0.01, β_1 was set to 0.9, β_2 to 0.999 and ε to 0.999). The Adam optimizer improves backpropagation such that each weight parameter is adapted according to its first and second momentum (Kingma and Ba, 2015). Each neural network was trained using 1000 epochs with a batch size of 100. The loss function was set to the mean squared error. To prevent overfitting, the training set was further split into train and validation set with 80 percent train. The validation dataset was then used for early stopping with a patience parameter of 10 epochs. The model with lowest validation error is then used for test set prediction. Due to poor performances, the inner cross validation was left out for the neural network training sequence. Neural Networks were implemented using the TensorFlow framework (Abadi *et al.*, 2016).

Gradient Boosted Trees using the XGBOOST Framework

A common problem with neural networks is the high dependency on the provided set of features and potential to learn spurious input-output associations. In this analysis a feature vector of all 8 frequency bands concatenated for 5 time points requires a Wiener Filter with 40 weights. In an architecture like neural networks all these features are contributing to the overall force prediction, nevertheless not all weight parameters are promising. Decision Tree algorithms overcome this problem naturally by implementing optimization of input feature use in their architecture. Thus, decision trees and random forests, first described by Breiman (Breiman, 2001), were proven to be a robust, accurate and successful tool for solving machine learning tasks, including classification, regression, density estimation and manifold learning or semi-supervised learning (Gall and Lempitsky, 2013). Random forests are an ensemble method consisting of many decision trees. A decision tree is a statistical optimal data segregation method, that is only controlled by conditional sequences. Different implementations were proposed on top of Decision Trees. AdaBoost (Schapire, 2009) is an adaptive learning algorithm that builds up successive decision trees iteratively. By that an ensemble of multiple weighted weak learners are combined to yield a strong estimator. Gradient Boosting is built using the same concept. According to Empirical Risk Minimization it fits each decision tree

based on the residuals of a defined objective function. This objective function is typically based on an error loss and a regularization term. The model is initialized using a constant value. In an iterative process the new trees are added to the model up till the maximum defined estimators are reached. Here the scalable tree boosting framework XGBOOST (Chen and Guestrin, 2016) was used. In this analysis the number of boosting rounds is set to 10. The depth of each tree is sampled uniformly in a range from 1 to 100. When adding new trees to the model the parameter learning rate η is scaling the contribution of each tree prediction and is sampled here log uniformly from of the range $[10^{-5}, 1]$. Regularization in Gradient Boosted Trees is controlled by different factors. One of the factors is the minimum splitting loss γ. For every decision tree new nodes were added only if the *gain* metric was above γ. It is here sampled from a uniform distribution between 1 and 10. Hyperparameters for all used machine learning methods are listed in detail in Supplementary File 1b.

Source Power Comodulation

A state of the art movement prediction approach is the source separating framework called Source Power Comodulation (SPoC) (Dähne *et al.*, 2014). Oscillatory sources are here extracted based on their power comodulation with the force gripping target. SPoC was implemented using the MNE framework (Gramfort *et al.*, 2013). Thus, discriminant neural sources are made visible. In this context, the band-power at each frequency band of interest was calculated by taking the logarithm of the variance of the projected signal in the source space. For sake of comparison, only one spatial filter was used for feature computation at each frequency band. In the same manner as before, a Wiener filter was then applied in order to resample time lags up to 500 ms. Here again, the band power features are then used as input features. A Bayesian Optimization hyperparameter search was also here implemented for both the enet model as well as the XGBOOST framework with the aforementioned parameters.

Hyperparameter Search: Bayesian Optimization

All models underwent an extensive hyperparameter search using Bayesian optimization. A common problem using machine learning algorithms is finding the optimal hyperparameter settings given a certain architecture. *Grid search* exhaustively tries out all provided hyperparameters while *Random search* only draws random parameters from the given hyperparameter distributions. Sampling the error loss function can be computationally expensive. Bayesian Optimization formulates this problem into an optimization problem. Here a cost function is minimized given a set of hyperparameters. Instead of sampling from the objective cost function, a probabilistic model is defined. The hyperparameters minimizing the negative expected improvement *are selected* given a multinomial Gaussian process *using a Matern kernel*. Those parameters are then used to sample from the respective regressor in the given dataset. The resulting error is used to update the gaussian process distribution and given the maximum expected improvement, the next best hyperparameter set is drawn. This process is repeated for the elastic net, *neural networks and* XGBOOST architecture for 10 iterations. For every round a 3 fold cross validation is used in order to prevent

775 overfitting. Given log-uniform distributions a wide range of hyperparameters can thus be sampled in a
776 computationally efficient manner. The implementation was done using the scikit-optimize framework
777 (https://scikit-optimize.github.io/stable/). *Supplementary File 1b* lists the hyperparameters subjected to
778 Bayesian optimization. The chosen methodology is non-exhaustive and primarily serves the comparison of
779 variance in decoding explained by the recording location of the signal (ECoG vs. STN), motor symptom
780 severity (UPDRS-III), beta bursts and brain networks. It further gives an intuition about the potential of more
781 complex and elaborate machine learning methods for brain computer interfaces.
782

783 ## Definition of best model and best channels
784

785 Previous studies have repeatedly demonstrated that using a single optimal channel in the STN is
786 advantageous over using all available channels (Shah *et al.*, 2018). Most importantly, addition of more
787 channels leads to decreased generalization and higher risk of overfitting with little performance benefit.
788 Based on these results and to account for varying numbers of available electrode contacts, one channel
789 with optimal decoding performance on the cross-validation test set was chosen per patient to quantify and
790 compare decoding performance for the ECoG and STN analysis across patients. Since hyperparameter
791 optimization is implemented only within each inner cross validation fold, any circularity and data leakage is
792 circumvented. A robust decoding performance estimate is thus obtained through left out testing data only.
793

794 ## Analysis of beta bursts during motor preparation and movement execution
795 ## periods
796

797 To investigate a potential relationship between grip-force decoding performance and beta burst activity, we
798 have adopted a previously validated approach to movement related burst analyses (Torrecillos *et al.*, 2018;
799 Lofredi *et al.*, 2019). Therefore, the beta feature time-series were used and a threshold constituting the 75th
800 percentile of the rest periods were calculated. Next, threshold crossings of at least 100 ms lengths in the
801 motor preparation (-1 to 0 s with respect to movement) and movement execution (0 to 1 s with respect to
802 movement execution) were marked as bursts. In previous reports, the most informative metric was the “time
803 spent in burst” which is calculated as the sum of burst durations in the time period of interest. This metric is
804 directly proportional to the burst probability at a given time-point. All burst analyses were repeated for the
805 low-beta and high-beta bands in ECoG and STN-LFP. The times spent in bursts were correlated with
806 UPDRS-III and ECoG based decoding performances.
807

808 ## Prediction Network Mapping with whole-brain connectomics
809

810 To investigate whether decoding performance from different recording locations can cross-predict decoding
811 performances across patients, we developed a whole-brain connectomics based approach. Therefore,
812 ECoG electrode recording locations were projected to normative structural and functional MRI data
813 (Parkinson's Progression Markers Initiative [PPMI]; www.ppmi-info.org) using Lead-DBS software in Matlab

(www.lead-dbs.org).(Horn *et al.*, 2019) The PPMI connectomes of patients with PD (n = 74) was priorly computed (Ewert *et al.*, 2018) and has been used in context of DBS multiple times (Horn, Neumann, *et al.*, 2017; Neumann *et al.*, 2018; de Almeida Marcelino *et al.*, 2019; Lofredi *et al.*, 2021). No patient specific diffusion or functional MRI was required for this analysis. Seeding from each recording site resulted in connectivity profiles (fingerprints) that were expressed as voxel-wise whole-brain volumes for functional and structural connectivity and a set of streamline connections for structural connectivity. We have adapted three previously published methods leveraging normative connectomes as predictive models.

First, fiber streamlines representative of structural connectivity between ECoG channels and all other brain areas were isolated and assigned with a "Fiber T-score", associating XGBOOST decoding performance with the fiber tracts connectivity from respective ECoG recording locations across patients using mass-univariate two-sample t-tests between R^2 scores in connected vs. unconnected recording locations. Only fibers with significant t-scores surviving FDR correction at an alpha level 0.05 were considered further. Next, T-values were used as weights in an aggregated fiber score to predict out of training sample channel and patients' performances. Next, functional connectivity maps were used to generate an "R-Map", a connectivity model which is associated with optimal decoding performance, by performing voxel-wise correlations of connectivity and decoding performance from recording locations. The connectomic fingerprint from each recording location can then be assigned a spatial correlation coefficient that may have predictive value for the underlying decoding performance. The predictive value of these two methods were confirmed using "leave-one-channel-out" and "leave-one-subject-out" cross-validation. Finally, statistical parametric mapping was used to confirm the described correlations of structural and functional connectivity using linear-mixed effects models. In a voxel-wise approach, structural connectivity between ECoG channels and all other brain areas was calculated using Lead Mapper (www.lead-dbs.org). Statistical voxel-wise correlation between decoding performance and structural and functional connectivity, separate mixed effects models, with a subject based random effect, were corrected for multiple comparisons with random field theory as implemented in the Statistical parametric mapping (SPM12) toolbox (https://www.fil.ion.ucl.ac.uk/spm/). Functional connectivity strengths between recording sites and sensorimotor cortex (peak coordinate x = -38, y = -22, z = 72), parietal lobe (x = 6, y = -32, z = 82), striatum (x = -34, y = -24, z = 26) and cerebellum (x = 18, y = -50, z = -50 and x = -22, y = -52, z = -54) accounted for decoding performance. Similarly, for structural connectivity, a significant cluster in the sensorimotor region (x = -44, y = -18, z = 70) correlated with high decoding performance. All connectivity analyses were performed using ECoG recording locations with contralateral R^2 performances (Figure 1E). A schematic illustrating the different steps of functional and structural prediction network mapping can be found in Figure 7-figure supplement 1.

Statistical Analysis

Results are stated as mean ± standard deviation. All significance testing was performed using two-sided Monte-Carlo permutation tests and bootstrapping. P-values were obtained by shuffling value positions and determining the resulting original rho value percentile in the distribution of surrogate combinations. Spearman's correlations were performed because of small sample size and varying distributions. Clinical correlations were performed using preoperative UPDRS-III total scores. To test for the temporal specificity of the clinical correlation with decoding performance, we performed sample-wise correlations of decoding output with UPDRS-III total scores across subjects. Multiple comparisons were corrected by adjusting the significance threshold α to the false discovery rate (Benjamini and Hochberg, 2000).

Data availability

The original raw data can be made available after definition and institutional signatures on data sharing agreements in accordance to data privacy protection and data governance laws. The code and data for the reproduction of every Figure, machine learning and statistical analysis are openly available at the GitHub repository (https://github.com/neuromodulation/icn/tree/master/ECOG_vs_STN).

Funding

The present manuscript was supported through a US-German Collaborative Research in Computational Neuroscience (CRCNS) grant to R.S.T., R.M.R. and W.J.N. with funding from the German Federal Ministry for Research and Education and NIH (R01NS110424). Further funding was provided through Deutsche Forschungsgemeinschaft (DFG, German Research Foundation) – Project-ID 424778371 – TRR 295 to A.H. and W.J.N.

A.H. was supported by the German Research Foundation (Deutsche Forschungsgemeinschaft, Emmy Noether Stipend 410169619 and 424778371 – TRR 295) as well as Deutsches Zentrum für Luft- und Raumfahrt (DynaSti grant within the EU Joint Programme Neurodegenerative Disease Research, JPND).

Some data used in the preparation of this article were obtained from the PPMI database (www.ppmi-info.org/data). For up-to-date information on the study, visit www.ppmi-info.org. PPMI, a public–private partnership, is funded by the Michael J. Fox Foundation for Parkinson's Research. For funding partners, see www.ppmi-info.org/fundingpartners.

Supplementary Figure Legends

Figure 1-figure supplement 1: Analyzed movements show variability in maximum amplitude and velocity. (A) All used normalized and baseline corrected grip force traces. (B) Maximum peak amplitude histogram (C) All movement trace velocities.

Figure 7-figure supplement 1: "Prediction Network Mapping" allows for prediction of machine learning decoding performances using functional and structural connectivity. (A) Functional connectivity "Fingerprints" are estimated using fMRI resting state correlations of the Volume of Tissue Activated (VTA) voxels correlation to all other voxels. (B) The correlation of every fingerprint voxel values and their respective R^2 decoding performances allow for calculation of the optimal connectivity profile for maximum decoding performance called "R-MAP". (C) The R-MAP correlation with individual fingerprints of cross validation left out channels, or set of channels for single subjects, allows for prediction of decoding performance. High correlation with the R-MAP optimal connectivity predicts high decoding performance. (D) Structural connectivity can be used for decoding performance prediction. For all fibers a two sample t-test estimates a t value of connected and unconnected decoding performance contacts. The fiber t-value can thus be predictive of decoding performance.

Supplementary File 1 Legends

Supplementary File 1a: Electrode Details
Supplementary File 1b: Bayesian Optimization Hyperparameters
Supplementary File 1c: Best channel R^2 performances

References

Abadi, M. *et al.* (2016) 'TensorFlow: A system for large-scale machine learning', *Proceedings of the 12th USENIX Symposium on Operating Systems Design and Implementation, OSDI 2016* [Preprint].

Alhourani, A. *et al.* (2020) 'Subthalamic Nucleus Activity Influences Sensory and Motor Cortex during Force Transduction', *Cerebral Cortex*, 30(4), pp. 2615–2626. doi:10.1093/cercor/bhz264.

de Almeida Marcelino, A.L. *et al.* (2019) 'Subthalamic neuromodulation improves short-term motor learning in Parkinson's disease', *Brain*, 142(8), pp. 2198–2206. doi:10.1093/brain/awz152.

Androulidakis, A.G. *et al.* (2007) 'Dopaminergic therapy promotes lateralized motor activity in the subthalamic area in Parkinson's disease', *Brain*, 130(2), pp. 457–468. doi:10.1093/brain/awl358.

Appelhoff, S. *et al.* (2019) 'MNE-BIDS: Organizing electrophysiological data into the BIDS format and facilitating their analysis', *Journal of Open Source Software*, 4(44), p. 1896. doi:10.21105/joss.01896.

Arlotti, M. *et al.* (2018) 'Eight-hours adaptive deep brain stimulation in patients with Parkinson disease', *Neurology*, 90(11), pp. e971–e976. doi:10.1212/WNL.0000000000005121.

924 Baldermann, J.C. *et al.* (2019) 'Connectivity Profile Predictive of Effective Deep Brain Stimulation
925 in Obsessive-Compulsive Disorder', *Biological Psychiatry*, 85(9), pp. 735–743.
926 doi:10.1016/j.biopsych.2018.12.019.

927 Benjamini, Y. and Hochberg, Y. (2000) 'On the Adaptive Control of the False Discovery Rate in
928 Multiple Testing With Independent Statistics', *Journal of Educational and Behavioral Statistics*,
929 25(1), pp. 60–83. doi:10.3102/10769986025001060.

930 Beudel, M. and Brown, P. (2016) 'Adaptive deep brain stimulation in Parkinson's disease',
931 *Parkinsonism & Related Disorders*, 22 Suppl 1, pp. S123-126.
932 doi:10.1016/j.parkreldis.2015.09.028.

933 Blankertz, B. *et al.* (2006) 'The Berlin Brain-Computer Interface: Machine Learning Based
934 Detection of User Specific Brain States.', *Journal of Universal Computer Science*, 12, p.
935 581Â 607.

936 Brainard, D.H. (1997) 'The Psychophysics Toolbox', *Spatial Vision*, 10(4), pp. 433–436.
937 doi:10.1163/156856897X00357.

938 Breiman, L. (2001) 'Random forests', *Machine Learning* [Preprint].
939 doi:10.1023/A:1010933404324.

940 Cagnan, H. *et al.* (2019) 'Emerging technologies for improved deep brain stimulation', *Nature*
941 *Biotechnology*, 37(9), pp. 1024–1033. doi:10.1038/s41587-019-0244-6.

942 Caire, F. *et al.* (2013) 'A systematic review of studies on anatomical position of electrode
943 contacts used for chronic subthalamic stimulation in Parkinson's disease', *Acta Neurochirurgica*,
944 155(9), pp. 1647–1654; discussion 1654. doi:10.1007/s00701-013-1782-1.

945 Chen, T. and Guestrin, C. (2016) 'XGBoost: A Scalable Tree Boosting System', in *Proceedings of*
946 *the 22nd ACM SIGKDD International Conference on Knowledge Discovery and Data Mining*. New
947 York, NY, USA: Association for Computing Machinery (KDD '16), pp. 785–794.
948 doi:10.1145/2939672.2939785.

949 Cole, S.R. *et al.* (2017) 'Nonsinusoidal Beta Oscillations Reflect Cortical Pathophysiology in
950 Parkinson's Disease', *The Journal of Neuroscience: The Official Journal of the Society for*
951 *Neuroscience*, 37(18), pp. 4830–4840. doi:10.1523/JNEUROSCI.2208-16.2017.

952 Cole, S.R. and Voytek, B. (2017) 'Brain Oscillations and the Importance of Waveform Shape'.

953 Cruz, A.V. *et al.* (2009) 'Effects of Dopamine Depletion on Network Entropy in the External
954 Globus Pallidus', *Journal of Neurophysiology*, 102(2), pp. 1092–1102.
955 doi:10.1152/jn.00344.2009.

Dähne, S. *et al.* (2014) 'SPoC: a novel framework for relating the amplitude of neuronal oscillations to behaviorally relevant parameters', *NeuroImage*, 86, pp. 111–122. doi:10.1016/j.neuroimage.2013.07.079.

Dale, A.M., Fischl, B. and Sereno, M.I. (1999) 'Cortical surface-based analysis: I. Segmentation and surface reconstruction', *NeuroImage* [Preprint]. doi:10.1006/nimg.1998.0395.

Ewert, S. *et al.* (2018) 'Toward defining deep brain stimulation targets in MNI space: A subcortical atlas based on multimodal MRI, histology and structural connectivity', *NeuroImage*, 170, pp. 271–282. doi:10.1016/j.neuroimage.2017.05.015.

Feldmann, L.K. *et al.* (2021) 'Subthalamic beta band suppression reflects effective neuromodulation in chronic recordings', *European Journal of Neurology*, 28(7), pp. 2372–2377. doi:10.1111/ene.14801.

Fischer, P. *et al.* (2020) 'Movement-related coupling of human subthalamic nucleus spikes to cortical gamma', *eLife*. Edited by N.C. Swann, L.L. Colgin, and N.C. Swann, 9, p. e51956. doi:10.7554/eLife.51956.

Frazier, P.I. (2018) 'A Tutorial on Bayesian Optimization', *arXiv preprint arXiv:1012.2599* [Preprint].

Gall, J. and Lempitsky, V. (2013) *Decision Forests for Computer Vision and Medical Image Analysis*, *Decision Forests for Computer Vision and Medical Image Analysis*.

Geman, S., Bienenstock, E. and Doursat, R. (1992) 'Neural Networks and the Bias/Variance Dilemma', *Neural Computation* [Preprint]. doi:10.1162/neco.1992.4.1.1.

Gilron, R. *et al.* (2021) 'Long-term wireless streaming of neural recordings for circuit discovery and adaptive stimulation in individuals with Parkinson's disease', *Nature Biotechnology*, pp. 1–8. doi:10.1038/s41587-021-00897-5.

Gramfort, A. *et al.* (2013) 'MEG and EEG data analysis with MNE-Python', *Frontiers in Neuroscience*, 7. doi:10.3389/fnins.2013.00267.

Gunduz, A. *et al.* (2016) 'Differential roles of high gamma and local motor potentials for movement preparation and execution', *Brain-Computer Interfaces*, 3(2), pp. 88–102. doi:10.1080/2326263X.2016.1179087.

Haufe, S. *et al.* (2014) 'On the interpretation of weight vectors of linear models in multivariate neuroimaging', *NeuroImage*, 87, pp. 96–110. doi:10.1016/j.neuroimage.2013.10.067.

He, S. *et al.* (2021) 'Closed-Loop Deep Brain Stimulation for Essential Tremor Based on Thalamic Local Field Potentials', *Movement Disorders*, 36(4), pp. 863–873. doi:10.1002/mds.28513.

de Hemptinne, C. *et al.* (2015) 'Therapeutic deep brain stimulation reduces cortical phase-amplitude coupling in Parkinson's disease', *Nature Neuroscience*, 18(5), pp. 779–786. doi:10.1038/nn.3997.

Hirschmann, J. *et al.* (2013) 'A direct relationship between oscillatory subthalamic nucleus–cortex coupling and rest tremor in Parkinson's disease', *Brain*, 136(12), pp. 3659–3670. doi:10.1093/brain/awt271.

Hirschmann, J. *et al.* (2017) 'Parkinsonian rest tremor can be detected accurately based on neuronal oscillations recorded from the subthalamic nucleus', *Clinical Neurophysiology*, 128(10), pp. 2029–2036. doi:10.1016/j.clinph.2017.07.419.

Holdgraf, C. *et al.* (2019) 'iEEG-BIDS, extending the Brain Imaging Data Structure specification to human intracranial electrophysiology', *Scientific Data*, 6(1), p. 102. doi:10.1038/s41597-019-0105-7.

Horn, A., Reich, M., *et al.* (2017) 'Connectivity Predicts deep brain stimulation outcome in Parkinson disease', *Annals of Neurology*, 82(1), pp. 67–78. doi:10.1002/ana.24974.

Horn, A., Kühn, A.A., *et al.* (2017) 'Probabilistic conversion of neurosurgical DBS electrode coordinates into MNI space', *NeuroImage*, 150, pp. 395–404. doi:10.1016/j.neuroimage.2017.02.004.

Horn, A., Neumann, W.-J., *et al.* (2017) 'Toward an electrophysiological "sweet spot" for deep brain stimulation in the subthalamic nucleus', *Human Brain Mapping*, 38(7), pp. 3377–3390. doi:10.1002/hbm.23594.

Horn, A. *et al.* (2019) 'Lead-DBS v2: Towards a comprehensive pipeline for deep brain stimulation imaging', *NeuroImage*, 184, pp. 293–316. doi:10.1016/j.neuroimage.2018.08.068.

Horn, A. and Fox, M.D. (2020) 'Opportunities of connectomic neuromodulation', *NeuroImage*, 221, p. 117180. doi:10.1016/j.neuroimage.2020.117180.

Hwang, B.Y. *et al.* (2020) 'Perspective: Phase Amplitude Coupling-Based Phase-Dependent Neuromodulation in Parkinson's Disease', *Frontiers in Neuroscience*, 14, p. 558967. doi:10.3389/fnins.2020.558967.

Kehnemouyi, Y.M. *et al.* (2021) 'Modulation of beta bursts in subthalamic sensorimotor circuits predicts improvement in bradykinesia', *Brain*, 144(2), pp. 473–486. doi:10.1093/brain/awaa394.

Khawaldeh, S. *et al.* (2020) 'Subthalamic nucleus activity dynamics and limb movement prediction in Parkinson's disease', *Brain*, 143(2), pp. 582–586. doi:10.1093/brain/awz417.

Kingma, D.P. and Ba, J.L. (2015) 'Adam: A method for stochastic optimization', in *3rd International Conference on Learning Representations, ICLR 2015 - Conference Track Proceedings*.

1022 Kondylis, E.D. *et al.* (2016) 'Movement-related dynamics of cortical oscillations in Parkinson's
1023 disease and essential tremor', *Brain: A Journal of Neurology*, 139(Pt 8), pp. 2211–2223.
1024 doi:10.1093/brain/aww144.

1025 Krauss, J.K. *et al.* (2021) 'Technology of deep brain stimulation: current status and future
1026 directions', *Nature Reviews. Neurology*, 17(2), pp. 75–87. doi:10.1038/s41582-020-00426-z.

1027 Kühn, A.A. *et al.* (2004) 'Event-related beta desynchronization in human subthalamic nucleus
1028 correlates with motor performance', *Brain*, 127(4), pp. 735–746. doi:10.1093/brain/awh106.

1029 Kühn, A.A. *et al.* (2006) 'Reduction in subthalamic 8-35 Hz oscillatory activity correlates with
1030 clinical improvement in Parkinson's disease', *The European Journal of Neuroscience*, 23(7), pp.
1031 1956–1960. doi:10.1111/j.1460-9568.2006.04717.x.

1032 Leuthardt, E.C. *et al.* (2004) 'A brain-computer interface using electrocorticographic signals in
1033 humans', *Journal of Neural Engineering*, 1(2), pp. 63–71. doi:10.1088/1741-2560/1/2/001.

1034 Li, N. *et al.* (2020) 'A unified connectomic target for deep brain stimulation in obsessive-
1035 compulsive disorder', *Nature Communications*, 11(1), p. 3364. doi:10.1038/s41467-020-16734-
1036 3.

1037 Little, S. *et al.* (2013) 'Adaptive deep brain stimulation in advanced Parkinson disease', *Annals of*
1038 *Neurology*, 74(3), pp. 449–457. doi:10.1002/ana.23951.

1039 Little, S. *et al.* (2019) 'Human motor cortical beta bursts relate to movement planning and
1040 response errors', *PLOS Biology*, 17(10), p. e3000479. doi:10.1371/journal.pbio.3000479.

1041 Lofredi, R. *et al.* (2018) 'Dopamine-dependent scaling of subthalamic gamma bursts with
1042 movement velocity in patients with Parkinson's disease', *eLife*, 7. doi:10.7554/eLife.31895.

1043 Lofredi, R. *et al.* (2019) 'Beta bursts during continuous movements accompany the velocity
1044 decrement in Parkinson's disease patients', *Neurobiology of Disease*, 127, pp. 462–471.
1045 doi:10.1016/j.nbd.2019.03.013.

1046 Lofredi, R. *et al.* (2021) 'Subthalamic stimulation impairs stopping of ongoing movements',
1047 *Brain*, 144(1), pp. 44–52. doi:10.1093/brain/awaa341.

1048 Mallet, N. *et al.* (2008) 'Disrupted Dopamine Transmission and the Emergence of Exaggerated
1049 Beta Oscillations in Subthalamic Nucleus and Cerebral Cortex', *Journal of Neuroscience*, 28(18),
1050 pp. 4795–4806. doi:10.1523/JNEUROSCI.0123-08.2008.

1051 Mayka, M.A. *et al.* (2006) 'Three-dimensional locations and boundaries of motor and premotor
1052 cortices as defined by functional brain imaging: a meta-analysis', *NeuroImage*, 31(4), pp. 1453–
1053 1474. doi:10.1016/j.neuroimage.2006.02.004.

1054 Mehring, C. *et al.* (2004) 'Comparing information about arm movement direction in single
1055 channels of local and epicortical field potentials from monkey and human motor cortex', *Journal*
1056 *of Physiology-Paris*, 98(4–6), pp. 498–506. doi:10.1016/j.jphysparis.2005.09.016.

1057 Merk, T. *et al.* (2022) 'Machine learning based brain signal decoding for intelligent adaptive
1058 deep brain stimulation', *Experimental Neurology*, 351, p. 113993.
1059 doi:10.1016/j.expneurol.2022.113993.

1060 Milosevic, L. *et al.* (2018) 'Neuronal inhibition and synaptic plasticity of basal ganglia neurons in
1061 Parkinson's disease', *Brain*, 141(1), pp. 177–190. doi:10.1093/brain/awx296.

1062 Molina, R. *et al.* (2021) 'Closed-Loop Deep Brain Stimulation to Treat Medication-Refractory
1063 Freezing of Gait in Parkinson's Disease', *Frontiers in Human Neuroscience*, 15.
1064 doi:10.3389/fnhum.2021.633655.

1065 Neumann, W. and Rodriguez-Oroz, M.C. (2021) 'Machine Learning Will Extend the Clinical Utility
1066 of Adaptive Deep Brain Stimulation', *Movement Disorders*, 36(4), pp. 796–799.
1067 doi:10.1002/mds.28567.

1068 Neumann, W.-J. *et al.* (2016) 'Subthalamic synchronized oscillatory activity correlates with
1069 motor impairment in patients with Parkinson's disease', *Movement Disorders*, 31(11), pp. 1748–
1070 1751. doi:10.1002/mds.26759.

1071 Neumann, W.-J. *et al.* (2019) 'Toward Electrophysiology-Based Intelligent Adaptive Deep Brain
1072 Stimulation for Movement Disorders', *Neurotherapeutics: The Journal of the American Society*
1073 *for Experimental NeuroTherapeutics*, 16(1), pp. 105–118. doi:10.1007/s13311-018-00705-0.

1074 Neumann, W.-J.J. *et al.* (2018) 'Functional segregation of basal ganglia pathways in Parkinson's
1075 disease', *Brain*, 141(9), pp. 2655–2669. doi:10.1093/brain/awy206.

1076 Opri, E. *et al.* (2020) 'Chronic embedded cortico-thalamic closed-loop deep brain stimulation for
1077 the treatment of essential tremor.', *Science translational medicine*, 12(572).
1078 doi:10.1126/scitranslmed.aay7680.

1079 Pedregosa, F. *et al.* (2011) 'Scikit-learn: Machine learning in Python', *Journal of Machine*
1080 *Learning Research* [Preprint].

1081 Pernet, C., Wilcox, R. and Rousselet, G. (2013) 'Robust Correlation Analyses: False Positive and
1082 Power Validation Using a New Open Source Matlab Toolbox', *Frontiers in Psychology*, 3, p. 606.
1083 doi:10.3389/fpsyg.2012.00606.

1084 Peterson, S.M. *et al.* (2021) 'Generalized neural decoders for transfer learning across
1085 participants and recording modalities', *Journal of Neural Engineering*, 18(2), p. 026014.
1086 doi:10.1088/1741-2552/abda0b.

1087 Petrucci, M.N. *et al.* (2020) 'Neural closed-loop deep brain stimulation for freezing of gait', *Brain*
1088 *Stimulation*, 13(5), pp. 1320–1322. doi:10.1016/j.brs.2020.06.018.

1089 Piña-Fuentes, D., van Dijk, J.M.C. and M, B. (2019) 'Adaptive DBS in Parkinson's disease:
1090 Headlines, perspectives and challenges', *Brain Stimulation*, 12(4), pp. 1091–1092.
1091 doi:10.1016/j.brs.2019.04.014.

1092 Proakis, J.G. and Monolakis, D.G. (1996) *Digital signal processing: principles, algorithms, and*
1093 *applications*, *Pentice Hall*.

1094 Randazzo, M.J. *et al.* (2016) 'Three-dimensional localization of cortical electrodes in deep brain
1095 stimulation surgery from intraoperative fluoroscopy', *NeuroImage* [Preprint].
1096 doi:10.1016/j.neuroimage.2015.10.076.

1097 Rosset, A., Spadola, L. and Ratib, O. (2004) 'OsiriX: An open-source software for navigating in
1098 multidimensional DICOM images', *Journal of Digital Imaging* [Preprint]. doi:10.1007/s10278-
1099 004-1014-6.

1100 Schapire, R.E. (2009) 'A Short Introduction to Boosting', *Society* [Preprint]. doi:10.1.1.112.5912.

1101 Schwerdt, H.N. *et al.* (2020) 'Dopamine and beta-band oscillations differentially link to striatal
1102 value and motor control', *Science Advances*, 6(39), p. eabb9226. doi:10.1126/sciadv.abb9226.

1103 Shah, S.A. *et al.* (2018) 'Towards Real-Time, Continuous Decoding of Gripping Force From Deep
1104 Brain Local Field Potentials.', *IEEE transactions on neural systems and rehabilitation*
1105 *engineering : a publication of the IEEE Engineering in Medicine and Biology Society*, 26(7), pp.
1106 1460–1468. doi:10.1109/TNSRE.2018.2837500.

1107 da Silva, J.A. *et al.* (2018) 'Dopamine neuron activity before action initiation gates and
1108 invigorates future movements', *Nature*, 554(7691), pp. 244–248. doi:10.1038/nature25457.

1109 Starr, P.A. (2018) 'Totally Implantable Bidirectional Neural Prostheses: A Flexible Platform for
1110 Innovation in Neuromodulation', *Frontiers in Neuroscience*, 12. doi:10.3389/fnins.2018.00619.

1111 Swann, N.C. *et al.* (2018) 'Adaptive deep brain stimulation for Parkinson's disease using motor
1112 cortex sensing', *Journal of neural engineering*, 15(4), p. 046006. doi:10.1088/1741-2552/aabc9b.

1113 Tan, H. *et al.* (2016) 'Decoding gripping force based on local field potentials recorded from
1114 subthalamic nucleus in humans', *eLife*, 5. doi:10.7554/eLife.19089.

1115 Thenaisie, Y. *et al.* (2022) 'Principles of gait encoding in the subthalamic nucleus of people with
1116 Parkinson's disease'. medRxiv, p. 2022.02.08.22270370. doi:10.1101/2022.02.08.22270370.

1117 Tinkhauser, G. *et al.* (2017) 'The modulatory effect of adaptive deep brain stimulation on beta
1118 bursts in Parkinson's disease', *Brain: A Journal of Neurology*, 140(4), pp. 1053–1067.
1119 doi:10.1093/brain/awx010.

1120 Tinkhauser, G. and Moraud, E.M. (2021) 'Controlling Clinical States Governed by Different
1121 Temporal Dynamics With Closed-Loop Deep Brain Stimulation: A Principled Framework',
1122 *Frontiers in Neuroscience*, 15. Available at:
1123 https://www.frontiersin.org/article/10.3389/fnins.2021.734186 (Accessed: 18 March 2022).

1124 Torrecillos, F. *et al.* (2018) 'Modulation of Beta Bursts in the Subthalamic Nucleus Predicts
1125 Motor Performance', *The Journal of Neuroscience: The Official Journal of the Society for*
1126 *Neuroscience*, 38(41), pp. 8905–8917. doi:10.1523/JNEUROSCI.1314-18.2018.

1127 Turner, R.S. and Desmurget, M. (2010) 'Basal ganglia contributions to motor control: a vigorous
1128 tutor', *Current Opinion in Neurobiology*, 20(6), pp. 704–716. doi:10.1016/j.conb.2010.08.022.

1129 Velasco, S. *et al.* (2022) 'The Entropy of Adaptively Segmented Beta Oscillations Predict Motor
1130 Improvement in Patients with Parkinsons Disease', *IEEE Transactions on Biomedical Engineering*,
1131 pp. 1–1. doi:10.1109/TBME.2022.3142716.

1132 Velisar, A. *et al.* (2019) 'Dual threshold neural closed loop deep brain stimulation in Parkinson
1133 disease patients', *Brain Stimulation*, 12(4), pp. 868–876. doi:10.1016/j.brs.2019.02.020.

1134 Wilson, L.E., Castanheira, J. da S. and Baillet, S. (2022) 'Time-resolved parameterization of
1135 aperiodic and periodic brain activity'. bioRxiv, p. 2022.01.21.477243.
1136 doi:10.1101/2022.01.21.477243.

1137 Xie, Z., Schwartz, O. and Prasad, A. (2018) 'Decoding of finger trajectory from ECoG using deep
1138 learning', *Journal of Neural Engineering*, 15(3), p. 036009. doi:10.1088/1741-2552/aa9dbe.

1139 Yttri, E.A. and Dudman, J.T. (2016) 'Opponent and bidirectional control of movement velocity in
1140 the basal ganglia', *Nature*, 533(7603), pp. 402–406. doi:10.1038/nature17639.

1141 Zou, H. and Hastie, T. (2005) 'Regularization and variable selection via the elastic net', *Journal of*
1142 *the Royal Statistical Society. Series B: Statistical Methodology* [Preprint]. doi:10.1111/j.1467-
1143 9868.2005.00503.x.

1144